# Loss of the volume-regulated anion channel components LRRC8A and LRRC8D limits platinum drug efficacy

Carmen A Widmer[1], Ismar Klebic[1,2], Natalya Domanitskaya[1], Morgane Decollogny[1], Denise Howald[1], Myriam Siffert[1], Paul Essers[3], Zuzanna Nowicka[4], Nadine Stokar-Regenscheit[1], Marieke van de Ven[5], Renske de Korte-Grimmerink[5], José A Galván[6], Colin E J Pritchard[7], Ivo J Huijbers[7], Wojciech Fendler[4,8], Conchita Vens[3,9], Sven Rottenberg[1,10,11,12]

**Affiliations:**

[1]Institute of Animal Pathology, Vetsuisse Faculty, University of Bern, 3012 Bern, Switzerland; [2]COMPATH, Institute of Animal Pathology, Vetsuisse Faculty, University of Bern, 3012 Bern, Switzerland; [3]Department of Radiation Oncology, The Netherlands Cancer Institute, Amsterdam, The Netherlands; [4]Department of Biostatistics and Translational Medicine, Medical University of Lodz, 92-215 Lodz, Poland; [5]Mouse Clinic for Cancer and Aging Research (MCCA), Preclinical Intervention Unit, The Netherlands Cancer Institute, 1066CX Amsterdam, The Netherlands; [6]Translational Research Unit, Institute of Pathology, University of Bern, Bern, Switzerland; [7]Mouse Clinic for Cancer and Aging Research (MCCA), Transgenic Facility, The Netherlands Cancer Institute, 1066CX Amsterdam, The Netherlands; [8]Department of Radiation Oncology, Dana-Farber Cancer Institute, Boston, MA 02215, USA; [9]Department of Head and Neck Oncology and Surgery, The Netherlands Cancer Institute, Amsterdam, The Netherlands; [10]Division of Molecular Pathology, The Netherlands Cancer Institute, 1066CX Amsterdam, The Netherlands; [11]Bern Center for Precision Medicine, University of Bern, 3012 Bern, Switzerland; [12]Cancer Therapy Resistance Cluster, Department for BioMedical Research, University of Bern, 3012 Bern, Switzerland

**Running title:** LRRC8A and LRRC8D affect platinum drug efficacy

**Keywords:** VRAC, LRRC8A, LRRC8D, Platinum drug resistance, BRCA1, high-dose chemotherapy, genetically engineered mouse model, breast cancer, HNSCC

**Financial support:** Swiss National Science Foundation (310030_179360 to S.R.), the European Research Council (ERC-2019-AdG-883877 to S.R.), the Swiss Cancer League (KLS-4282-08-2017 to S.R.), and the Wilhelm-Sander Foundation (no. 2019.069.1 to S.R.)

**Corresponding author**: Sven Rottenberg, Länggassstrasse 122, 3012 Bern, Switzerland, +41 31 6842395, sven.rottenberg@vetsuisse.unibe.ch

**Conflict of interest:** The authors declare no potential conflicts of interest.

**Abstract**

In recent years platinum (Pt) drugs have been found to be especially efficient to treat patients with cancers that lack a proper DNA damage response, *e.g.* due to dysfunctional BRCA1. Despite this knowledge, we are still missing helpful markers to predict Pt response in the clinic. We have previously shown that volume-regulated anion channels, containing the subunits LRRC8A and LRRC8D, promote the uptake of cisplatin and carboplatin in BRCA1-proficient cell lines. Here, we show that the loss of LRRC8A or LRRC8D significantly reduces the uptake of cis- and carboplatin in BRCA1;p53-deficient mouse mammary tumor cells. This results in reduced DNA damage and *in vivo* drug resistance. In contrast to *Lrrc8a*, the deletion of the *Lrrc8d* gene does not affect the viability and fertility of mice. Interestingly, *Lrrc8d*$^{-/-}$ mice tolerate a two-fold cisplatin maximum-tolerable dose. This allowed us to establish a mouse model for intensified Pt-based chemotherapy, and we found that an increased cisplatin dose eradicates BRCA1;p53-deficient tumors, whereas eradication is not possible in WT mice. Moreover, we show that decreased expression of *LRRC8A/D* in head and neck squamous cell carcinoma patients, who are treated with a Pt-based chemoradiotherapy, leads to decreased overall survival of the patients. In particular, high cumulative cisplatin dose treatments lost their efficacy in patients with a low *LRRC8A/D* expression in their cancers. Our data therefore suggest that LRRC8A and LRRC8D should be included in a prospective trial to predict the success of intensified cis- or carboplatin-based chemotherapy.

## Statement of significance

We demonstrate that lack of expression of *Lrrc8a* or *Lrrc8d* significantly reduces the uptake and efficacy of cis- and carboplatin in Pt-sensitive BRCA1;p53-deficient tumors. Moreover, our work provides support to confirm the *LRRC8A* and *LRRC8D* gene expression in individual tumors prior to initiation of intensive platinum-based chemotherapy.

## Introduction

For over 40 years platinum (Pt) compounds have been used as major components of chemotherapy regimens for several types of cancer (1). Even in the era of precision medicine and immunotherapy, Pt drugs remain among the most widely used anti-cancer drugs, due to their efficacy. (2). Especially for cancer types in which the use of immune checkpoint inhibitors has been disappointing thus far, like ovarian cancer (3), Pt drugs are a mainstay of current therapy. Moreover, Pt-based chemotherapy may enhance the success of immunotherapy as shown for lung cancer as well as head and neck squamous cell carcinoma (HNSCC) (4,5). In Pt drug research, it is well established that DNA is the major cellular target (6). The three most frequently used Pt drugs in the clinic — cisplatin, carboplatin and oxaliplatin — all affect normal DNA functions by generating mono-adducts as well as intra- and interstrand DNA crosslinks (2), subsequently leading to cell death in case these adducts remain unresolved. Consistent with this finding, Pt drugs synergize with tumors that show defects in the DNA damage response (DDR) (7). A useful example is breast cancer. Platinum drugs are not a standard treatment for breast cancer, since their efficacy on most forms of breast cancer is modest. However, patients with breast carcinomas that are defective in DNA repair by homologous recombination (HR) due to the lack of function of BRCA1, BRCA2 or other repair proteins in the HR pathway, do benefit from platinum-based chemotherapy (8–11). We also observed this in a genetically engineered *K14cre;Brca1$^{F/F}$;Trp53$^{F/F}$* (KB1P) mouse model for *BRCA1*-mutated breast cancer. The *Brca1$^{-/-}$;Trp53$^{-/-}$* mammary tumors were highly sensitive to cis- or carboplatin (12,13).

Although HR deficiency scores provide useful information for patient stratification, the lack of additional reliable biomarkers for the prediction of Pt-based chemotherapy response still represents a major clinical limitation (2,14). Despite the long use of platinum drugs, precision medicine approaches to tackle this challenge are still in their infancy. Moreover, those patients with disseminated tumors who show a major initial response usually develop secondary drug resistance. The precise mechanisms of Pt drug resistance remain poorly defined (2,15,16). One mechanism that has been confirmed in patients with *BRCA1*- or *BRCA2*-mutated cancers is the occurrence of secondary mutations in the *BRCA1* or *BRCA2* genes, leading to HR restoration (17,18). Nevertheless, this mechanism alone does not explain all cases of secondary resistance (19) and it is less suitable for predicting upfront therapy response of patients with HR-defective tumors who receive their initial anti-cancer therapy. In the past, a major focus of the drug resistance studies was put on active Pt drug influx or efflux using tumor cell lines selected *in vitro*

with platinum drugs. However, no transporter has been unambiguously linked to clinical platinum drug resistance thus far (15,20).

In addition to transporters and diffusion, channels provide another route for platinum drugs to penetrate the cell membrane. Using genome-wide functional genetic screens for platinum drug resistance in haploid cells, we have identified volume-regulated anion channels (VRACs), composed of leucine-rich repeat containing (LRRC)8A and LRRC8D plasma membrane proteins, as the long sought-after plasma membrane entry points for cis- and carboplatin (21). VRACs, consisting of LRRC8 hexamers, contribute to the cellular volume regulation. The release of cellular solutes such as chloride and potassium ions reduces cell swelling under hypotonic conditions (22,23). For successful formation of the hexameric channel structure at the plasma membrane, the subunit LRRC8A is obligatory, as its knockout abolishes chloride currents even when the other paralogs (LRRC8B-E) are overexpressed (22,24). The composition of the other subunits (LRRC8B-E) are thought to determine the channel substrate specificity.

As the functional data on the role of LRRC8A and LRRC8D in platinum drug resistance is based on HR-proficient tumor cell lines thus far (21), we set out to study their role in the HR-deficient KB1P model. Indeed, loss of *Lrrc8a* or *Lrrc8d* in KB1P tumors largely abrogated the high Pt drug sensitivity of these tumors *in vitro* and *in vivo*, even though the uptake of cis- or carboplatin was reduced only by about 50% in LRRC8A- or LRRC8D-deficient *Brca1*$^{-/-}$*;Trp53*$^{-/-}$ cells. Using *Lrrc8d*$^{-/-}$ mice we show that intensified platinum therapy does eradicate KB1P tumors, whereas we are unable to do so in WT mice. Moreover, we corroborate the relevance of *LRRC8A* and *LRRC8D* gene expression for intensified Pt therapy in HNSCC patients.

## Methods

### Lead contact and material availability

Further information and requests for resources and reagents should be directed to and will be fulfilled by the Lead Contact, Sven Rottenberg (sven.rottenberg@vetsuisse.unibe.ch).

### 2D and 3D cell culture

For the 2D cell culture we used the cisplatin-sensitive, *Brca1*-mutated KB1PM5_control1 cell line, which we previously established (25). Cells were grown in Dulbecco's Modified Eagle Medium/Nutrient Mixture F-12 (DMEM/F12; Gibco, Thermo Scientific Cat#10565018) supplemented with 10% fetal calf serum (FCS; Biowest Cat#S1810-500), 50 units/ml penicillin-streptomycin (Gibco, Thermo Scientific Cat#15070063), 5µg/ml Insulin (Sigma Cat#I0516), 5 ng/ml cholera toxin (Sigma Cat#C8052) and 5 ng/ml murine epidermal growth-factor (EGF; Sigma Cat#E4127). Tissue culture of BRCA-deficient cell lines was carried out under low oxygen conditions (37°C, 5% CO2; 3% O2). Testing for mycoplasma contamination was performed twice per year using PlasmoTest (InvivoGen Cat#rep-pt1).

The KB1P4N 3D tumor organoid line was previously established from a *Brca1*$^{-/-}$*;Trp53*$^{-/-}$ mouse mammary tumor and cultured as described (26). Briefly, cultures were embedded in Cultrex Reduced Growth Factor Basement Membrane Extract Type 2 (BME; Trevigen Bio-Techne Cat#3533-010010) (40µL BME:growth media 1:1 drop in a single well of 24-well plate) and grown in Advanced DMEM/F12 (AdDMEM/F12, Gibco Cat#11550446) supplemented with 1M HEPES (Sigma Cat#H0887), GlutaMAX (Gibco Cat#35050061) 50 U/ml penicillin-streptomycin (Gibco Cat#A9165), B27 (Gibco Cat#17504044), 125µM N-acetyl-L-cysteine (Sigma Cat#A9165) and 50ng/ml murine epidermal growth factor (Sigma Cat#E4127). Organoids were cultured under standard conditions (37°C, 5% CO2) and regularly tested for mycoplasma contamination. Before transplantation, organoids were tested for pathogen contamination by IDEXX BioAnalytics services. For all cell cultures, testing for mycoplasma contamination was performed twice per year using PlasmoTest (InvivoGen Cat#rep-pt1). 2D and 3D KB1P cell lines were authenticated by a specific genotyping PCR for the introduced *Brca1* and *p53* mutations (25).

### Genome editing, plasmids and cloning

Generation of CRISPR/Cas9 plasmids was performed using a modified version of the pX330 backbone (Addgene Cat#42230) into which a puromycin resistance ORF was cloned under the hPGK promoter (27) for 2D cell lines or the lentiCRISPRv2 backbone (Addgene Cat#52961, RRID:Addgene_52961) for

the 3D organoids. The sgRNA sequences (Supplementary table 1) were cloned in the backbones using custom DNA oligos with the corresponding overhangs (Microsynth), which were melted at 95°C for 5 min, annealed at RT for 2h and subsequently ligated with quick-ligase (NEB Cat#M2200S) into BbsI (NEB Cat#R0539) digested pX330 or BsmBI-digested (Fermentas Cat#FD0454) lentiCRISPRv2 backbone. Sanger sequencing verified the correctness of all constructs' sequences.

LRRC8A and LRRC8D–deficient 2D cell lines were generated by transfection with pX330 vectors containing gRNAs targeting the respective genes. In brief, KB1PM5 cells were transfected with 2.5µg of plasmid DNA using the Mirus TransIT-LT1 reagent (Mirus Cat#MIR2300) and the corresponding protocol. Selection was performed using puromycin (Gibco, Thermo Scientific Cat#A1113802) at a concentration of 3µg/ml for 72 hours after transfection. Monoclonal cell lines were isolated by dilution of single cells per well into 96-well plates. Clones bearing big deletion mutations, created by pairing sgRNAs to target the same gene, were identified by gel electrophoresis resolution of PCR amplicons corresponding to edited loci (amplicon primer sequences below). Sanger sequencing also confirmed the gene disruption. Amplicon primers for *Lrrc8a*: FW: 5'-ACAGAGCTCCGCTACTTTGC-3' and RV: 5'-GGATGGTCACGTCGGGTATC-3', amplicon primers for *Lrrc8d*: FW: 5'-CCCTTGCGGAAGTTGCTTCA-3' and RV: 5'-CAGCTCCTGCTTATCCTGGG-3'

**Genomic DNA isolation, PCR amplification and TIDE analysis**

To determine the modification rate of cell populations which had been transfected/transduced using individual sgRNA targeting the gene of interest, the gene region was sequenced and analyzed using the Tracking of Indels by Decomposition (TIDE) tool. In brief, cells were pelleted and genomic DNA was extracted using the QIAmp DNA mini kit (Qiagen Cat#51306) according to manufacturer's protocol. Target loci were amplified using Phusion High Fidelity Polymerase (Thermo Scientific Cat#F530L) using following conditions: (1) 98 °C, 30 s, (2) 30 cycles of 98 °C for 10 s, 63.8 (*Lrrc8a*) or 64.2 (*Lrrc8d*) °C for 20 s and 72 °C for 30 s, (3) 72 °C, 5 min. The reaction mix consisted of 10µl of 2x Phusion Mastermix 1µl of 10µM forward and reverse primer and 100ng of DNA in 20µl total volume. PCR products were purified using the QIAquick PCR purification kit (Qiagen Cat#28104) according to manufacturer's protocol. Subsequently, the PCR product was submitted to Sanger sequencing with the corresponding forward primers (listed below). Target modification rate was determined from the chromatogram (.ab1) sequence using the TIDE algorithm (28). For *Lrrc8a* sgRNA3 amplicon: FW: 5'-GGCCATT-

GGTGGGGTTCTTA-3' and RV: 5'-GGTGCGTGGAAACTTGAACC -3' (product size 550 bp), sequencing Primer: FW: 5'-ACAGAGCTCCGCTACTTTGC-3', For *Lrrc8d* sgRNA2 amplicon: FW: 5'-AAAGGGTTCTCATTGGTCCCAC-3' and RV: 5'-CGCCTTAGTTGTCCAGGGAG-3' (product size 730 bp), sequencing primer: FW: 5'-AGGGAGGGCCAGATGGTAAC-3'.

**Reconstitution of *Lrrc8a/d* cDNA**

*Lrrc8a* or *Lrrc8d* reconstitution was performed using a modified version of the pOZ-N-FH-IL2Rα plasmid (kindly provided by Dipanjan Chowdhury, Harvard Medical School, USA). Briefly, the vector backbone was amplified using the following primers, which excluded the FLAG and HA tags from the original vector from the linearized vector PCR product: FW: 5'-TCGAGAGATCCGGGAGACACAA-3' and RV: 5'-CTCGAGCGGAAGATCTGGCAGTCT-3'. The *Lrrc8a* or *Lrrc8d* coding sequence was amplified from freshly prepared cDNA by primers including the C-terminal Myc sequence and corresponding plasmid overlaps suited for subsequent cloning using the in-fusion HD cloning kit by Takara Bio (Takara Cat#12141). *Lrrc8a* FW: 5'-GATCTTCCGCTCGAGATGATTCCGGTGACAGAGCTCCGC-3' and RV: 5'-TTGTGTCTCCCGGATCTCTCGATGCGGCCCTACAGATCCTCTTCTGAGATGAGTTTTTGTTCTC-CTCCAGCGGCCGCGGCCTGCTCCTTGTCAGCTC-3' *Lrrc8d* FW: 5'-GATCTTCCGCTCGAGATG-TTTACCCTTGCGGAAGTTGC-3' and RV: 5'-TTGTGTCTCCCGGATCTCTCGATGCGGCCCTACAGA-TCCTCTTCTGAGATGAGTTTTTGTTCTCCTCCAGCGGCCGCAATCCCGTTTGCAAAGGGGACA-3'. Correct cDNA insertion was verified by Sanger sequencing of the complete open reading frames. Fifty percent confluent phoenix retrovirus producer cells (Gentaur Molecular Products Cat#RVK-1001, RRID:CVCL_H717) were transfected with pOZ-*Lrrc8a*-Myc, pOZ-*Lrrc8d*-Myc or empty pOZ-Myc using Turbofectin transfection reagent (Origene, LabForce Cat#TF81001). The next day, virus-containing supernatant was collected, filtered through a 0.45µm filter before application to LRRC8A or LRRC8D –deficient monoclonal target cells. 8µg/ml Polybrene (Merck Millipore Cat#TR-1003-G) was added to each target cell dish. Virus was harvested and applied to target cells on three consecutive days. IL2Rα –expressing cells were selected using magnetic beads coated with a CD25 antibody (Dynabeads CD25; Thermo Scientific Cat#11157D).

**Lentiviral transduction of organoids**

Lentiviral stocks were generated by transient transfection of HEK293FT cells, which we obtained from ThermoFischer (Cat#R70007; RRID:CVCL_6911). On day 0, $8x10^6$ HEK293FT cells were seeded in 150cm$^2$ cell culture dishes and on the next day transiently transfected with lentiviral packaging plasmids

and the plentiCRISPRv2 vector containing the respective sgRNA (*Lrrc8a* sgRNA 3 or *Lrrc8d* sgRNA2) or a non-targeting sgRNA using 2xHBS (280nM NaCl, 100mM HEPES, 1.5mM Na2HPO4, pH 7.22), 2.5M $CaCl_2$ and 0.1x TE buffer (10mM Tris pH8.0, 1mM EDTA pH8.0, diluted 1:10 with dH2O). After 30h, virus-containing supernatant was concentrated by ultracentrifugation at 20.000rpm for 2h in a SW40 rotor at 4°C and the virus was finally resuspended in 100µL PBS. The virus titer was determined using a qPCR Lentivirus Titration Kit (Applied Biological Materials Cat#LV900). Tumor-derived organoids were transduced according to a previously established protocol (26). The target sites modifications of the polyclonal cell pools were analyzed by TIDE analysis as described previously.

**Clonogenic assays**

For clonogenic growth assays in a 6-well plate (TPP Cat#92406) format, 2000 KB1PM5 cells were seeded per well in DMEM-F12 complete medium. 24 hours after seeding, the cells were treated with the indicated drug doses over the course of 24h. After 8 days, the wells were fixed with 4% PFA/PBS and stained with 0.1% crystal violet. Quantification of the wells was performed with ImageJ using the ColonyArea plugin (version 1.53i) (29).

**Growth assays**

For growth assays, KB1PM5 cells were seeded to 96-well plates (TPP Cat#92696) at a density of 100 cells per well. Proliferation was measured on seven consecutive days using CellTiter-Blue® Cell Viability Assay (Promega Cat#G9241) following manufacturer's instructions.

**Competition assays**

The polyclonal cell pools generated by transfection with individual sgRNAs targeting either *Lrrc8a* or *Lrrc8d* were used for competition assays. In brief, cells were seeded to 12-well plates (TPP Cat#92412) at 1000 cells/well and drug selection using different Pt-based agents was applied at indicated concentrations for 24 hours. After 8 days of recovery, cells were either fixed with PFA and stained with crystal violet (Figure S3D) or harvested and the gDNA isolated and processed for subsequent TIDE analysis as described previously.(28) The shift of mutated alleles was determined by comparing the modification rates of drug naïve and drug selected polyclonal cell populations.

## Western Blotting

Cells were washed and scraped in cold PBS. After pelleting, cells were lysed in RIPA buffer (50mM Tris-HCl pH 7.4; 1% NP-40; 0.5% Na-deoxycholate; 0.1% SDS; 150mM NaCl, 2nM EDTA, 50mM NaF) containing 1x complete protease inhibitor cocktail (Roche Cat#04693132001) for 60 minutes on ice, followed by homogenization via syringe and needle. The lysate was subsequently cleared by centrifugation for 10 minutes at 14.000 rpm. Protein concentrations of the supernatants were determined using the Pierce BCA assay kit (Thermo Scientific Cat#23225) with a BSA standard curve. Protein lysates were denatured at 70°C for 10 minutes in SDS sample buffer (Laemmli SDS sample buffer, reducing (6x); Thermo Scientific Cat#J61337.AC) and separated by SDS-PAGE on 7.5% acrylamide gels before overnight wet transfer for 18h at 15V to 0.45µm pore size PVDF membranes (GE Healthcare Cat#10600018). Membranes were blocked in 5% BSA in TBS-T (100 mM Tris, pH 7.5, 0.9% NaCl, 0.05% Tween-20) and subsequently incubated with primary antibodies diluted 1:1000 (anti-LRRC8A rabbit polyclonal, Bethyl Laboratories Cat#A304-175A, RRID:AB_2621424, anti-LRRC8A, anti-LRRC8D rabbit polyclonal provided by T. Jentsch) or 1:2000 (anti-beta Actin, mouse monoclonal Sigma Cat#A1978, RRID: AB_476697 and anti-alpha tubulin, mouse monoclonal Sigma Cat#T5168, RRID: AB_477579) in blocking buffer at 4°C overnight. After washing in TBS-T, Horseradish Peroxidase (*HRP*)-linked secondary antibodies diluted 1:2500 (anti-mouse IgG and anti-rabbit IgG, Cell Signaling Cat#7076, RRID:AB_330924, and Cat#7074, RRID:AB_10684258, respectively) were applied for 2h at room temperature. Images were acquired using the FUSION FX7 imaging system (Vilber GmbH).

## *In vivo* validation of resistance

All animal experiments were approved by the Animal Ethics Committee of The Netherlands Cancer Institute (Amsterdam, The Netherlands) and the Animal Ethics Committee of the canton of Bern (Switzerland) and are in accordance with the current Dutch and Swiss Acts on Animal Experimentation. CRISPR-Cas9-modified organoid lines derived from *K14cre; Brca1F/F;Trp53F/F* (KB1P) female mice were transplanted in 6-9 weeks-old NU/J nude mice (strain ID 3484) for the *in vivo* validation. The *Lrrc8a* or *Lrrc8d* modification rate in the outgrown tumors (N=6 each) was determined by TIDE analysis as described previously. Tumors with high modification rate percentage were chosen for the *in vivo* validation experiments.

For tumor piece transplantation, DMSO-frozen tumor pieces were thawed, washed with PBS, cut into small pieces and transplanted in the fourth right mammary fat pad of 6-9 week-old NMRI nude mice.

Mammary tumor size was measured by caliper measurements and tumor volume was calculated (length x width$^2$ / 2). Animals were randomly assigned to the treatment groups. Treatment of tumor bearing mice was initiated, when tumors reached a size of ~75 mm$^3$. Carboplatin (Teva Cat#6985451) was administered at 50 mg/kg intravenously over the course of two cycles (14 days between treatments). Animals were sacrificed with $CO_2$, when the tumor reached a volume of 1500 mm$^3$. Animal technicians who were blinded regarding the hypothesis performed tumor size measurements and treatments.

**Generation of *Lrrc8d* knockout mice**

The *Lrrc8d* conditional knockout mice were generated by an established CRISPR/Cas9-mediated gene editing protocol (30). Briefly, LoxP sites were introduced to flank the first coding exon of the *Lrrc8d* gene sequence (exon 3). Zygotes isolated from FVB mice were co-injected with a microinjection mix containing *in vitro* transcribed Cas9 mRNA, two sgRNAs targeting the different sites in the *Lrrc8d* gene (5'–CACCGGCTTCAGGATTCGGTAAGT-3' and 5'–CACCGCAGGCACACCCACGTGCGG-3') and two homology-directed repair oligos, each containing a LoxP site. Zygotes that have further divided into two-cell embryos after overnight incubation at 37°C, 5% CO2, were surgically implanted into the oviduct of a pseudopregnant foster mother. Correct incorporation of the LoxP sites was confirmed by PCR. Subsequently these mice were crossed with Cre recombinase expressing FVB mice, resulting in offspring with a 2,561 bp deletion in exon 3 of the *Lrrc8d* gene. Gene disruption was confirmed by PCR and the decrease in *Lrrc8d* expression levels was determined by RTqPCR and Western Blotting. Primer for *Lrrc8d* deletion genotyping PCR: FW: 5'-TTTCAGGAATGTTTACCCTTGCGG-3' and RV: 5'-TGCATCGTGTCCTGTTTAAAGGGC-3' (PCR product size if positive: 156 bp), Primer for wild type PCR: FW: 5'-TTTCAGGAATGTTTACCCTTGCGG-3' and RV: 5'-GGTGTGTGGCTGTTTCCATCCTG-3' (PCR product size if positive: 270 bp).

**RTqPCR of *Lrrc8d* mice**

For the expression determination of *Lrrc8d* using RTqPCR, a mastermix containing FastStart Universal SYBR Green Master Mix (Roche Cat#4913850001), forward and reverse primers at a final concentration of 300nM and water was prepared. 11µl of this mastermix were mixed with 4µl of cDNA template dilution (final dilution of 5ng/µl of cDNA in reaction) in a MicroAmp® Fast Optical 96-Well Reaction Plate (Thermo Scientific Cat#4343906) to subsequently be subjected to following PCR program: (1) 95 °C, 10 min, (2) 40 cycles of 95 °C for 10 s, 58°C 30 s, melting curve on a ABI 7500Fast device (Thermo Scien-

tific Cat#4406985). Expression levels are displayed relative to the *Hprt* housekeeping gene control expression. *Lrrc8d* Primer pair 1: FW: 5'-CTG CCT CTA CAC TCT CTT CTG GC-3' and RV: 5'-CGC AAA GTC GTT CTT GAC ATC CG-3'. *Lrrc8d* Primer pair 2: FW: 5'-CTG ACA TAC CTC TCC AAG CCA CC-3' and RV: 5'-GTC TCT CTT CTC CTT CTT CGC CT-3'. *Hprt* Primer pair: FW: 5'-CCT AAG ATG AGC GCA AGT TGA A-3' and RV: 5'-CCA CAG GAC TAG AAC ACC TGC TAA-3'.

**LRRC8D protein levels in mouse kidneys**

To determine the LRRC8D protein levels in wild type, heterozygous, and homozygous knockout mice, protein was isolated from whole kidneys by metal bead homogenization in PBS and subsequent lysis in T-PER Tissue Protein Extraction Reagent (Thermo Scientific Cat#78510) and 1x Halt protease inhibitor cocktail (Thermo Scientific Cat#87786). 80µg protein was subjected to electrophoresis and Western blotting. Antibody incubations using the rabbit anti-LRRC8D polyclonal antibody provided by T. Jentsch and subsequent imaging were performed as described previously.

**Cisplatin adduct and yH2AX IHC staining of mouse kidneys after treatment**

Littermate wild type, heterozygous, and homozygous *Lrrc8d* knockout mice were *i.v.* treated with 6mg cisplatin per kg (Teva Cat#4333164). After 6 hours, the animals were anesthetized with isoflurane, sacrificed with $CO_2$ followed by organ harvest. Kidneys of vehicle or cisplatin treated mice were fixed in 4% PFA and further embedded in paraffin. Each paraffin block was sectioned at 2.5µm and immunohistochemistry (IHC) was performed on an automated immunostainer (Leica Bond RX, Leica Biosystems Cat#95735-848538). The following antibodies were used for immunohistochemical staining of tumors: the home-made NKI-A59 antibody for the detection of cisplatin DNA-adducts as described previously (31) and the Phospho-Histone H2A.X Ser139 20E3 Rabbit mAb (Cell Signaling Cat#9718, RRID:AB_2118009) for the detection of yH2AX foci. Then all samples were incubated with HRP (Horseradish Peroxidase)-polymer for 15 min and subsequently visualized using 3,3'-Diaminobenzidine (DAB) as a brown chromogen (Bond polymer refine detection, Leica Biosystems, Cat#DS9800, RRID:AB_2891238) for 10 min. The samples were counterstained with hematoxylin for 5 min, dehydrated and mounted with Pertex (Sakura). Slides were scanned on a Panoramic 250 Flash scanner (3DHISTECH).

The percentage of positive nuclei in 50 kidney cortex image sections per kidney (for NKI-A59 antibody) using ImageJ (version 1.53i) or the whole cortical kidney region of each mouse (for yH2AX) determined

by QuPath v0.3.0 were quantified and normalized via the average basal levels of the vehicle treated samples. Numbers of animals per group, vehicle: wt N=5, het KO N=8, hom KO N=8; treated: wt N=8, het KO N=12, hom KO N=16. The data represent the normalized mean percentage of positive nuclei of all the image sections per mouse ± SD (two-way ANOVA, followed by Tukey's multiple comparisons test). A pathologist who was blinded concerning the sample identity carried out the quantification of both stainings.

**Imaging Mass Cytometry (IMC) measurement of Pt content in the kidneys**

The same kidney samples as for the Pt-adduct antibody IHC stainings were used for the IMC analysis. 3 kidneys of either cisplatin-treated or untreated wild type or homozygous LRRC8D-deficient mice underwent direct Pt-content analysis. Briefly, FFPE sections of 3.5um thickness on Superfrost TM Plus slides were dewaxed by Xylol and rehydrated stepwise by 100%, 94% and 70% Ethanol. Samples were washed with PBS and incubated with a 1:100 dilution of 25µM Ir-Intercalator (Fluidigm, Cat#201192A) for 30 min at RT to stain the nuclei. The samples were dipped three times in distilled water and air-dried before IMC analysis. The stained and dried samples were then inserted into the HyperionTM Imaging System (Standard BioTools [formerly Fluidigm], evolved from that described by Giesen, *et al*.(32)), where the tissue was ablated by a 1µm diameter UV laser. Tissue from an ablation spot was vaporized with each laser shot, and the plume containing the heavy metals present in the tissue was transported into the inductively coupled plasma ion source for detection. All data were acquired using the CyTOF software version 7.0.8493. Three 1mm$^2$ sections per kidney were acquired. For each image, the mean $^{194}$Pt, $^{191}$Ir, and $^{134}$Xe$^+$ values of three image sections were quantified. The mean $^{194}$Pt values were subsequently normalized by the background $^{134}$Xe$^+$ signal as described by Chang, *et al*. (33). The data represent the normalized mean $^{194}$Pt signal of the image sections ± SD (two-way ANOVA, followed by Tukey's multiple comparisons test).

**Drug toxicity in *Lrrc8d* KO mice**

To determine the tolerability of higher cisplatin doses, littermate wild type and homozygous *Lrrc8d* knockout mice were subjected to 6, 9, or 12 mg cisplatin per kg *i.v.* on day 0 and day 14. The body weight and physical state of the mice were monitored daily. The groups consisted of 5 animals each. Animals, where the bodyweight decreased below 90% of the starting weight before treatment were euthanized.

Cisplatin-resistant KB1P tumors were generated by repeated *i.p*. administration of 4mg cisplatin per kg to naïve KB1P tumors transplanted into FVB mice until no more treatment response was observed. This resulted in stably cisplatin resistant tumors. To test whether increased cisplatin doses could eradicate naïve and resistant tumors, tumor pieces were transplanted to the fourth mammary fat pat of FVB mice as described previously. The cisplatin naïve and resistant tumors were treated *i.v.* with two cycles of cisplatin starting from a size of ~ 150 $mm^3$ (day 0 and day 14). Tumor sizes were monitored for the succeeding 150 days post treatment. Animals with tumors reaching a volume of 1'000 $mm^3$ were sacrificed with $CO_2$. For the treatment with 12 mg/kg of cisplatin homozygous *Lrrc8d* knockout mice were used. Cisplatin naïve tumor groups: vehicle N=5, 6mg/kg N=10, 12 mg/kg N=5. Cisplatin resistant tumor groups: vehicle N=5, 6mg/kg N=5, 12 mg/kg N=5. Animal technicians who were blinded for the hypothesis of the treatment outcome conducted the tumor size measurements and treatments.

**Drug uptake measurement (CyTOF)**

KB1PM5 *Lrrc8a/d* wild type and knockout cell lines were seeded 2 days prior to drug treatment. It was aimed to have a starting cell number of 300'000 cells per condition at a density of 80% on treatment day. On the day of treatment, drug-containing medium was freshly prepared with the indicated concentrations and cells were treated for 3, 6, or 24 hours. After the treatment, cells were washed 3 times with serum containing culture medium for 5 minutes. Subsequently, cells were washed with room temperature PBS and then incubated with 0.25% Trypsin EDTA. Trypsinization was stopped with serum containing culture medium and the cells were then fully dissociated into a single-cell suspension by gentle pipetting. After dissociation, the cells were counted and 300'000 cells per condition were used for further fixation and barcoding according to the Cell-ID 20-plex Pd Barcoding kit (Fluidigm Cat#201060) protocol. Barcoded samples were then pooled and incubated with the Cell-ID intercalator Ir (Fluidigm Cat#201192A) at 100µl/ 1 Mio cells for 1h at room temperature and then stored at -80°C until measurement. For the measurement, samples were thawed, washed, mixed with equilibration beads and acquired on a Helios mass cytometer (Fluidigm). Post-acquisition, data was bead-normalized and debarcoded using the premessa R package released by the Parker Institute for Cancer Immunotherapy (https://github.com/ParkerICI/premessa). Absolute Pt- atom counts were determined by gating for Iridium$^{191}$ + BeadDist and $^{191}$Iridium +$^{193}$Irridium events to exclude cell debris, and $^{191}$Iridium + event length to exclude duplet signals using FlowJo version 10.8.1. Median Pt counts for the isotopes $^{192}$Pt, $^{194}$Pt, $^{195}$Pt, $^{196}$Pt, and $^{198}$Pt were summed to determine the total amount of Pt- atoms per cell. Data of a total

of 3 independent replicates consisting of 3 technical replicates each, where approximately 100'000 cells were acquired per condition are shown for figure 2A. For figure 2B and 2C three independent replicates, where approximately 50'000 cells were acquired per condition and replicate are shown. Statistical analysis was performed using GraphPad Prism 9 (2-way ANOVA followed by Tukey's multiple comparisons test).

**Immunofluorescence**

For the Cisplatin-DNA-adduct staining using the homemade NKI-459 antibody, 60'000 cells were seeded to 12 mm diameter coverslips (thickness Nr.1; Paul Marienfeld GmbH Cat#0111520). After 24 hours they were treated for the indicated durations with 10μM cisplatin. After treatment, the cells were washed with PBS and fixed with 4% PFA/PBS for 20 min at 4°C. Fixed cells were permeabilized for 20min in 0.5% Triton X-100/PBS, the DNA was denatured using 2M HCL for 10 min at 37°C. After washing with PBS, the cells were blocked in 1% BSA in PBS-T. The NKI-A59 antibody, diluted 1:200 in 1% BSA in PBS-T was applied for 2 h at room temperature. The secondary antibody Alexa Fluor 488 goat anti-rabbit IgG (Thermo Scientific Cat#A-11034, RRID: AB_2576217) was diluted 1:2000 in blocking buffer and incubated for 1h at room temperature. The DNA was stained with DAPI (Life Technologies Cat#D1306, 1:50000 dilution) before mounting onto positively charged microscopy slides using fluorescent mounting medium (Dako Cat#S3023). Analysis was performed on a DeltaVision Elite High Resolution Microscope system (GE Healthcare) consisting of an Olympus IX-70 inverted microscope with a CMOS camera, 100× Olympus Objective, and Softworx (Applied Precision, Issaquah, WA, USA) software. Per condition and replicate, approximately 100 cells from different areas of the coverslips were imaged in Z-stacks of 21 slices of 0.2μm thickness each. Images were analyzed using the FIJI image processing package of ImageJ (version 1.8.0) (34). Briefly, Z-stacks of the individual channels were projected using the "sum slices" projection. All nuclei were detected by the “analyze particles” command using the DAPI channel. This region of interest (ROI) selection was then used to determine the raw integrated density of the NKI-A59 antibody staining of each nucleus. ROI touching the edges of the images were excluded. Data were plotted in GraphPad Prism software 9 and significance was calculated using 2-way ANOVA followed by Tukey's multiple comparisons test.

For the γH2AX foci detection, the cells were seeded to coverslips, and treated with 2μM cisplatin for the indicated time points. After treatment, cells were washed with PBS and fixed with 4% PFA/PBS for 20 min at 4°C. Fixed cells were permeabilized for 20 min in 0.5% Triton X-100/PBS. All subsequent steps

were performed in staining buffer (PBS, BSA (2%), glycine (0.15%), Triton X-100 (0.1%)). Cells were washed 3 times and blocked for 30 min at RT using the described staining buffer. The cells were incubated overnight at 4°C with the primary antibody anti-phospho-Histone H2A.X (ser139) (clone JBW301, Merck Millipore Cat#05-636, RRID: AB_309864) at a dilution of 1:200 in staining buffer, washed 3 times and subsequently incubated with the secondary antibody Goat anti-Mouse IgG (H+L) Cross-Adsorbed Secondary Antibody Alexa Fluor (Thermo Scientific Cat#A-11029, RRID: AB_2534088) for 2 hours at RT. The coverslips were washed 5 times after secondary antibody staining, counterstained with DAPI as described previously and mounted onto positively charged Superfrost Plus Adhesion Microscope Slides (epredia Cat#J1800AMNZ) using fluorescence mounting medium (Dako Cat#S3023). Analysis was performed on a DeltaVision Elite High Resolution Microscope system (GE Healthcare) consisting of an Olympus IX-70 inverted microscope with a CMOS camera, 100× Olympus Objective, and SOFTWORX (Applied Precision, Issaquah, WA, USA) software. Per condition and replicate, approximately 200 cells from different areas of the coverslips were imaged in Z-stacks of 31 slices of 0.2µm thickness. Images were analyzed using the FIJI image processing package of ImageJ (version 1.8.0) (34). Briefly, Z-stacks of the individual channels were projected using the "max intensity" projection setting. All nuclei were detected by the “analyze particles” command using the DAPI channel projection and this ROI selection was then used to determine the number of yH2AX foci of each nucleus by the "finding maxima" command on the FITC channel. ROI touching the edges of the images were excluded. Data were plotted in GraphPad Prism 9 software and significance was calculated using ordinary one-way ANOVA followed by Tukey's multiple comparisons test.

**Statistical analysis HNSCC**

The collection of the HNSCC biopsies was approved by the Institutional Review Board of the Netherlands Cancer Institute. All patients signed an informed consent for the collection and analysis of the HNSCC samples and the study was conducted in accordance with International Ethical Guidelines for Biomedical Research Involving Human Subjects (CIOMS). CNV data of *LRRC8A* or *LRRC8D* was obtained by shallow DNA sequencing of head and neck squamous cell carcinomas dataset (35). Gene expression data was obtained by polyA RNA sequencing (36). Patients were classified into low or high *LRRC8A* expression by the cutoff at 20 rpkm.

**Statistical analysis ovarian cancer**

The GSE32063 dataset consists of 40 advanced-stage high-grade serous ovarian cancer samples. This study was performed after approval by the institutional review board. All patients provided a written informed consent for the collection and analysis of these samples and the study was conducted in accordance with International Ethical Guidelines for Biomedical Re-search Involving Human Subjects (CIOMS). All patients were treated with a combined platinum-taxane standard chemotherapy. Gene expression levels were obtained by whole human genome microarray sequencing (agilent- 014850 4x44K G4112F) (37). Patients were classified into low or high *LRRC8A* or *LRRC8D* expression by a cutoff of 33% (lower and upper tertile).

**Data availability statement**

The HNSCC dataset was previously published by Essers *et al.* (35). The Dutch multicenter cohort CNA and RNA-Seq data that support the findings of this study are available in the European Genome-Phenome Archive (EGA) at https://ega-archive.com under the EGA study numbers EGAS00001004090 (RNA-Seq data), EGAS00001004091 (low-coverage whole genome sequencing [WGS]) and data set numbers EGAD00001005716, EGAD00001005715 and EGAD00001005719, EGA D00001005718 for the RNA-Seq and low-coverage WGS, respectively.

The expression data of the ovarian cancer dataset was previously published by Yoshihara *et al*. and is available from Gene Expression Omnibus (GEO) data repository by the accession number GSE32063 (37).

## Results

### Loss of *Lrrc8a* or *Lrrc8d* induces cisplatin and carboplatin resistance in BRCA1;p53-deficient mouse mammary tumor cells

To investigate the effects of LRRC8A or LRRC8D defects on platinum drug sensitivity in HR-deficient tumors, we generated CRISPR/Cas9 knockouts in cell lines derived from a genetically engineered mouse model (GEMM) for hereditary *BRCA1*-mutated breast cancer (25). Due to the irreversible *Brca1* deletion these cells are highly sensitive to platinum drugs and thereby provide a useful tool to study mechanisms of Pt drug resistance that are independent of a restoration of BRCA1 function (38). Using a paired gRNA approach to generate big deletions in the *Lrrc8a* or *Lrrc8d* genes (Figure S1A+B), we obtained monoclonal cell lines that lost expression of LRRC8A (KB1PM5-*Lrrc8a*$^{-/-}$_C10, KB1PM5-*Lrrc8a*$^{-/-}$_D8) or LRRC8D (KB1PM5-*Lrrc8d*$^{-/-}$_E12, KB1PM5-*Lrrc8d*$^{-/-}$_G12) (Figure 1A). Knockout of *Lrrc8a* or *Lrrc8d* did not affect cell growth overall (Figure 1B). When we treated these *Lrrc8a*$^{-/-}$ and *Lrrc8d*$^{-/-}$ cells with cisplatin (Figure 1C+D) and carboplatin (Figure 1E+F), we observed an increased survival using clonogenic assays, the *Lrrc8a*$^{-/-}$ cells being more resistant than the *Lrrc8d*$^{-/-}$cells. In contrast, only a minor effect was observed in response to oxaliplatin in the LRRC8D-deficient cells (Figure 1G+H). Furthermore, we observed resistance of the knockout cell lines to the protein synthesis inhibitor blasticidin S (Figure S2A+B). The uptake of this drug is known to be LRRC8D-dependent (39). The reintroduction of the *Lrrc8a* cDNA (Figure S2C-E) re-sensitized the *Lrrc8a*$^{-/-}$ cells to both cis- and carboplatin as well as to blasticidin S in both polyclonal and monoclonal rescue lines, whereas no clear effect was detected for oxaliplatin (Figure 1I+J, Figure S2F-J). For the *Lrrc8d*$^{-/-}$ cell lines the reconstitution of the *Lrrc8d* cDNA also re-sensitized cells to cisplatin, carboplatin and blasticidin S (Figure 1K-M and Figure S2H+J), with only a minor effect for oxaliplatin (Figure S2I+J).

We further corroborated these data using polyclonal cells that we generated with single *Lrrc8a*- or *Lrrc8d*-targeting sgRNAs (Figure S3). With the help of the Tracking of Indels by Decomposition (TIDE) analysis (28), we quantified the presence of wild type and *Lrrc8a/d*-modified alleles in the polyclonal cell populations (Figure S3A+B). These polyclonal cell populations, that contain about 50% wild type alleles, were then treated with the Pt-based agents cisplatin, carboplatin, and oxaliplatin (Figure S3C). As expected by the presence of wild type alleles, the resistance to cis- and carboplatin was milder compared to the knockout clones presented in Figure 1 (Figure S3D). More importantly, when we measured the frequency of frameshift modifications following drug treatment, we observed a clear selection in favor of

the *Lrrc8a*- and Lrrc8*d*-mutated alleles following cis- and carboplatin. Regarding oxaliplatin, only for the *Lrrc8d*-mutated alleles we observed a modest positive selection when treating with the 0.5μM drug concentration (Figure S3E+F).

In our previous study using human HAP1 cells, we found that less carboplatin enters the cells if they contained VRACs that were LRRC8A- or LRRC8D-deficient (21). We also measured the Pt uptake in our *Lrrc8a*$^{-/-}$ and *Lrrc8d*$^{-/-}$ KB1PM5 cells using CyTOF, which allows the use of more physiological drug concentrations than were tested previously in the HAP1 cells. After incubation with 0.5μM of cisplatin or 4μM carboplatin for 24h, the Pt content was reduced by more than 65% in the *Lrrc8a*$^{-/-}$ cells for both cisplatin and carboplatin and about 25% for cisplatin and 35% for carboplatin in the *Lrrc8d*$^{-/-}$ cells (Figure 2A+B). The decrease could be reversed by the reintroduction of *Lrrc8a* or *Lrrc8d* (Figure 2C). The decrease in intracellular Pt-accumulation can be expected to result in less Pt-DNA adducts. To test this, we used the NKI-A59 antibody (31), which detects cisplatin-induced DNA adducts. Consistent with the uptake data, less Pt-DNA adducts were formed in the LRRC8A- and LRRC8D-deficient cells (Figure 2D+E). Again, the effect was stronger in the *Lrrc8a*$^{-/-}$ cells than the *Lrrc8d*$^{-/-}$ cells. The lower amount of Pt-DNA adducts resulted in less DNA damage, as measured by γH2AX foci formation (Figure 2F+G). Hence, the high cisplatin sensitivity of the BRCA1-deficient cells is alleviated in the absence of LRRC8A or LRRC8D, due to reduced drug uptake.

**LRRC8A and LRRC8D defects abrogate the *in vivo* efficacy of carboplatin**

Many clinicians prefer carboplatin to cisplatin, as the toxicity profiles of the two drugs differ, including a lower nephrotoxicity of carboplatin than cisplatin (40). To validate the role of LRRC8A and LRRC8D in the Pt-drug response *in vivo*, we tested the carboplatin response of the tumors in our breast cancer KB1P model, using the 3D organoid technology (26). For this purpose, KB1P4N organoids, derived from a *Brca1*$^{-/-}$*;Trp53*$^{-/-}$ mammary tumor (41), were transduced with lentiviruses carrying *Lrrc8a* or *Lrrc8d* targeting pLENTiCRISPRv2 vectors. Control organoids were generated by transduction with pLentiCRISPRv2, encoding a non-targeting sgRNA. LRRC8A/D-deficient organoids were then transplanted orthotopically into the mammary fat pad of mice. The outgrowing tumors were analyzed by TIDE and indeed showed a high frameshift modification percentage (Figure S4A-B). When the organoid-derived control or *Lrrc8a/d*-targeted tumors reached a volume of 75 $mm^3$, we treated them with the maximum tolerable dose (MTD) of 50mg/kg carboplatin *i.v.* on days 0 and 14 (Figure 3). The tumor volume was monitored throughout the whole experiment (Figures S4C-D). As shown in Figure 3, depletion of *Lrrc8a* or *Lrrc8d*

significantly lowered the tumor response to carboplatin and resulted in a decreased overall survival (*p*-value =0.002 for *Lrrc8a*, *p*-value =0.0131 for *Lrrc8d*) (Figure 3). Consistent with the *in vitro* data, the effect was stronger in the LRRC8A-deficient tumors than in the LRRC8D-deficient ones. These data demonstrate that loss of *Lrrc8a* or *Lrrc8d* renders BRCA1;p53-deficient tumors resistant to carboplatin *in vivo*.

**$Lrrc8d^{-/-}$ mice are viable and provide a useful model to study high-dose cisplatin therapy**

It was previously shown that *Lrrc8a* knockout mice are severely compromised and show an increased mortality *in utero* and postnatally (42). To test whether the *Lrrc8d* knockout is tolerable in mice, we introduced a large 2561 bp deletion of the protein coding sequence in exon 3 using CRISPR/Cas9-mediated gene editing of FVB/N zygotes (Figure 4A). This completely abrogated *Lrrc8d* expression at the RNA and protein level in homozygous mice, and also significantly reduced RNA and protein levels in heterozygous animals (Figure 4B and Figure S5A+B). In contrast to the *Lrrc8a* knockout mice, we did not see any alterations regarding fertility or histomorphology of the $Lrrc8d^{-/-}$ mice that we followed for at least 6 months. We therefore conclude that the $Lrrc8d^{-/-}$ mice are fully viable. In FVB/N mice, we previously reported an MTD of 6mg cisplatin per kg *i.v*. on days 0+14 (38). We could not escalate the dose above MTD levels by bone marrow reconstitution, and 3 days post treatment using 9mg/kg or 12mg/kg cisplatin *i.v.* the body weight dropped below 90% and animals had to be sacrificed. In contrast, in the $Lrrc8d^{-/-}$ mice we could double the dose to 12mg cisplatin per kg and the average weight of the mice stayed above 90% (Figure S5C). A main cytotoxic side effect of cisplatin is the increased death of tubular epithelial cells in the renal cortex. We therefore directly measured the Pt content in the kidneys of the *Lrrc8d*-proficient and homozygous knockout mice 6h after treatment with 6mg cisplatin per kg *i.v.* For the analysis, the amount of Pt was measured in three kidneys per group using imaging mass cytometry (IMC). The mean $^{194}Pt$ values per section were normalized to the $^{134}Xe^{+}$ background signal intensity. Indeed, the amount of Pt that we found in the kidneys of $Lrrc8d^{-/-}$ mice was lowered by about 50% compared to the wild type mice (Figure 4C+D). With less cisplatin entering the kidneys, we expected a reduction in the cisplatin-DNA adducts to be formed in the nuclei of tubular epithelial cells, which cause the nephrotoxicity. As presented in Figure S5D+E, these cells can be detected with the NKI-A59 antibody against Pt-DNA adducts 6h after treatment of wild type mice with 6mg cisplatin per kg *i.v*. The amount of Pt-DNA adducts was also substantially decreased in the kidneys of $Lrrc8d^{-/-}$ mice and to a lesser extent also in the $Lrrc8d^{+/-}$ animals, in comparison to the wild type mice (Figure 4E+F).

This decrease of Pt-DNA adducts correlated with a decrease in DNA damage, measured by γH2AX foci formation (Figure 4E+G). These data show that also *in vivo* less cisplatin enters LRRC8D-deficient cells.

Despite the high cisplatin sensitivity of the KB1P tumors, the tumors are not easily eradicated, not even with repeated treatments using the MTD (38). We previously showed that residual G0-like tumor cells that transiently avoid entering the cell cycle can escape the cisplatin-induced DNA damage, even without functional BRCA1 (38). The fact that *Lrrc8d*$^{-/-}$ mice tolerate the double MTD of the wild type mice allowed us to address the basic question whether a high dose of cisplatin eradicates the KB1P tumors containing functional VRACs. As shown in Figure 4H this is indeed the case. The KB1P donor tumor transplanted orthotopically into syngeneic wild type FVB/N relapsed after about 60 days following 6mg/kg cisplatin *i.v.* on days 0 and 14. In contrast, no tumor relapse was detected when the same KB1P tumor was transplanted orthotopically into syngeneic *Lrrc8d*$^{-/-}$ FVB/N mice and treated with 12mg/kg cisplatin *i.v*. on days 0 and 14. By applying repeated dosing of 4mg/kg cisplatin *i.p.* in wild type FVB/N mice (hence 2/3 of the MTD), we also managed to generate cisplatin-resistant KB1P tumors that showed stable resistance to 6mg/kg *i.v*. when transplanted into FVB/N mice (Figure 4I). Even these resistant tumors were eradicated using the high-dose therapy (12mg/kg) in *Lrrc8d*$^{-/-}$ mice. These data show that both sensitive and resistant *Brca1;Trp53*-deficient tumors cannot compensate the damage induced by high-dose cisplatin entering the tumor cells.

**Low expression of *LRRC8A* or *LRRC8D* correlates with decreased overall survival and reduced recurrence free survival in HNSCC patients treated with cisplatin-based chemoradiotherapy**

In the clinic, the use of platinum drugs for the treatment of BRCA-deficient breast cancer patients has only recently been expanded, and currently the sample availability for this specific subgroup is scarce. Another tumor type in which BRCA mutations are frequently found and which is highly sensitive to platinum-based chemotherapy is ovarian cancer. Using the TCGA and Patch *et al.* data sets, we have previously reported a lower survival of ovarian cancer patients who have a low *LRRC8D* gene expression (21). We could confirm this in another independent data set of ovarian cancer patients (GSE32063) (37). As shown in Figure S6, patients expressing low *LRRC8D* levels had a significantly decreased overall survival (*p*-value = 0.009) and non-significantly shortened progression-free survival (*p*-value = 0.096).

As the relevance of LRRC8A or LRRC8D function for platinum drug uptake is independent of BRCA1/2 status, we also studied LRRC8A/D in head and neck squamous cell carcinoma (HNSCC) patients, for

565 which cisplatin is a standard therapy in combination with radiotherapy (Figure 5). In contrast to the
566 ovarian cancer cohort, we had both copy number variation (CNV) and gene expression data available
567 from the tumors of these HNSCC patients. CNV analysis identified 20 out of 166 tumors with a loss of
568 the *LRRC8A* gene. In these patients, the loss of *LRRC8A* is associated with a lower overall survival
569 (OS, *p*-value =0.014) and increased tumor progression (*p*-value =0.028) compared. Moreover, the loss
570 of *LRRC8A* in these patients is correlated with an increased risk for failure of locoregional control (*p*-
571 value =0.0046) and distant metastasis (*p*-value =0.051) after treatment (Figure 5A). To test for
572 alterations in the level of *LRRC8A* transcripts, gene expression data of these patients was analyzed.
573 Samples were classified to low (<20 rpkm, N=58) and high (>20 rpkm, N=129) subgroups (Figure 5B).
574 Low *LRRC8A* gene expression correlated significantly with poor overall survival in these patients (*p*-
575 value = 0.0057) (Figure 5C).

576 It has previously been shown that patients benefit from cumulative cisplatin-based radiotherapy regi-
577 mens above 200mg/m$^2$ (43,44). We therefore stratified patients according to their cumulative dose, and
578 their overall survival was analyzed according to their *LRRC8A* expression levels (for low *LRRC8A* ex-
579 pression N=43 in ≥ 200mg/m$^2$ and N=24 in < 200 mg/m$^2$). The loss of *LRRC8A* expression resulted in
580 a decrease of the overall survival curves to the levels of lower and less effective cisplatin doses (Figure
581 5D). The data suggest that HNSCC patients with high *LRRC8A* expression are likely to benefit from
582 higher cisplatin doses.

583 Regarding *LRRC8D*, we also identified a group of 61 patients with low gene expression, and these
584 patients are different from those expressing low levels of *LRRC8A* (Figure 5E). The stratification of the
585 tumors into low (N=61), medium (N=60), and high (N=60) *LRRC8D* gene expression subgroups re-
586 vealed decreased overall survival (*p*-value =0.051) and poor tumor progression outcome (*p*-value=
587 0.054) in the low expression group. No effects on locoregional control of the tumor were found (*p*-value
588 = 0.84) (Figure 5 F). Moreover, low *LRRC8D* expression correlated with an increased distant metastasis
589 occurrence (*p*-value =0.030) (Figure 5G). To assess the impact of *LRRC8D* expression on varying cu-
590 mulative cisplatin doses, patients were split into ≥200 mg/m$^2$ and <200mg/m$^2$ receiving subgroups. Low
591 expression was defined as the lowest tertile expressing group in both treatment classes (N=37 in ≥
592 200mg/m$^2$ and N=23 in < 200 mg/m$^2$). Low *LRRC8D* gene expression was associated with increased
593 distant metastasis, especially in the ≥ 200mg/m$^2$ subgroup of patients (*p*-value=0.0054) (Figure 5H).
594 This association was strongest in the distant metastasis formation (Figure 5I).

Hence, in cisplatin-treated HNSCC patients, low *LRRC8A* and *LRRC8D* expression is associated with poor outcome. Based on our experimental work, this is explained by poor drug uptake of these tumors.

## Discussion

Using a mouse model for *BRCA1*-mutated breast cancer, we show here the relevance of LRRC8A- and LRRC8D-mediated cis- and carboplatin uptake to kill Pt drug-sensitive tumors. The potential relevance to the treatment of human cancer is suggested by our finding that ovarian cancer as well as HNSCC patients with low gene expression levels of *LRRC8A* or *LRRC8D* in their tumors have a reduced benefit of Pt-based chemotherapy. Hence, the absence of LRRC8A or LRRC8D in tumor cells may be a helpful marker to avoid the use of cis- or carboplatin.

At present, there is no biomarker routinely applied in the clinic to predict the outcome of Pt-based chemotherapy. In part, this may be due to the fact that cisplatin influx into tumor cells was long thought to be completely due to passive diffusion (15). Although active influx via SLC31A1 - the mammalian homolog of the budding yeast copper transporter (CTR1) - or via OCT2 (SLC22A2) - an organic cation transporter – was suggested, these transporters could not be unambiguously proven to cause reduced uptake and drug resistance when absent (45,46). OCT2 has been shown to mediate cisplatin-induced nephrotoxicity (47,48), but its expression is largely limited to the kidney, explaining why it may not be involved in tumor uptake. Decreased accumulation of platinum drugs may also be caused by increased drug export. In this context, two Cu transporters - ATP7A and 7B - were put forward (49). Despite some correlations that have been reported between poor cisplatin response and high ATP7B levels in patients, the role of these efflux transporters in Pt drug resistance remains to be clarified (2,15,20). Moreover, low-level cisplatin resistance was reported in cells overexpressing *MRP2*, but in human tumors, there is no consistent correlation between *MRP2* expression and cisplatin resistance (15,46). In summary, no transporter has been explicitly linked to clinical platinum drug resistance, be it importer or exporter (2,20).

In addition to diffusion or transporters, channels provide another route for platinum drugs to enter cells. Already in 1993 Gately and Howell (50) concluded that a fraction of cisplatin enters via a channel, because there are several inhibitors that decrease cisplatin entry. The authors suggest that about half of the cisplatin uptake is by passive diffusion through the membrane and the other half through a dedicated channel. More than 50% inhibition by any inhibitor has not been seen, resulting in this 50% channel estimate. Using genome-wide functional genetic screens for carboplatin drug resistance in human HAP1 cells, we have recently identified VRACs composed of LRRC8A and LRRC8D proteins as these long sought-after plasma membrane entry points for cis- and carboplatin (21). Loss of LRRC8D

was also a major hit in a genome-scale CRISPR–Cas9 knockout screen for cisplatin resistance using *BRCA1*-mutated ovarian cancer cells (51). Here, we confirm the relevance of these proteins for sensitivity to Pt drugs, using Pt drug-sensitive BRCA1;p53-deficient mouse mammary tumors and cell lines derived from this model. Despite their strong drug sensitivity due to an irreversibly deleted *Brca1* gene, the effect of cis- and carboplatin was largely abrogated in the absence of LRRC8A or LRRC8D. We found that about 50% of carbo- and cisplatin uptake depended on LRRC8A and LRRC8D (Figure 2), which is consistent with the assumption of Gately and Howell (50) and our observations in HAP1 cells (21). According to recent Cryo-EM studies of the LRRC8 subunits, the substrate specificity for larger osmolytes is likely dependent on the presence of LRRC8D in the channel composition. LRRC8D is the largest isoform, presenting the longest extracellular loop between transmembrane domain 1 and 2 (52,53). Of note, homo-hexameric LRRC8D structures contain a wider pore diameter than structures consisting of solely LRRC8A (53,54). Together with LRRC8A, LRRC8D seems to be responsible for the cellular uptake of Pt-based drugs, in contrast to the other subunits (LRRC8C, LRRC8E) (21). However, the effect of LRRC8A depletion on Pt drug resistance is not seen in all cell lines though, most likely because LRRC8A is essential for some of them (24,55). *Lrrc8a* knockout mice are severely compromised and show an increased mortality *in utero* and postnatally, as well as infertility (42,56). In contrast, we found that *Lrrc8d* knockout mice are viable and breed normally. Although further experiments are required to investigate Pt drug pharmacokinetics, renal excretion and nephrotoxicity, we clearly observed less cisplatin and Pt-DNA adducts in the kidneys of *Lrrc8d*$^{-/-}$ mice, resulting in reduced DNA damage. Due to reduced cisplatin uptake, their MTD is doubled, which allowed us to build a model for high-dose Pt drug-based chemotherapy. Both cisplatin-sensitive and –resistant LRRC8A- and LRRC8D-proficient KB1P tumors were completely eradicated when the cisplatin MTD was augmented two-fold (Figure 4). This is consistent with our previous findings using nimustine (38), that drug-tolerant cells can be eliminated, if sufficient damage is inflicted. Also in our cohort of HNSCC patients, the correlation between low *LRRC8A* or *LRRC8D* gene expression and poor cisplatin-based therapy response was more pronounced in the high dose groups. While further analyses need to be made to investigate whether this result can be reproduced using carboplatin, these data strongly indicate that it would be useful to assess the *LRRC8A* and *LRRC8D* expression of tumor cells before applying high dose cis- or carboplatin-based therapies. Clinicians might be able to avoid the serious side effects, if insufficient drug amounts can be expected to reach the tumor cell DNA, the main cellular target of platinum drugs. An alternative approach for cancers with low LRRC8A levels may be oxaliplatin. In our

KB1P model, we only observed a modest reduction in oxaliplatin uptake and consequent therapy resistance in *Lrrc8d*–deficient cells, suggesting oxaliplatin as useful alternative when patients are stratified based on *LRRC8A* expression.

Given the frequent use of Pt drugs in daily clinical practice, our data highlights the importance of further validation of LRRC8A and LRRC8D status as a predictive biomarker in prospective clinical trials. In addition to classical gene or protein expression correlations, our results also suggest the use of CyTOF-based measurements to quantitatively evaluate Pt uptake in patient-derived primary 2D or 3D cell cultures.

## Acknowledgments

We wish to thank Piet Borst, Diego Dibitetto, Martin Liptay, Marine Inglebert, and Lea Lingg for critical reading of the manuscript. Moreover, we thank the members of the Preclinical Intervention Unit of the Mouse Clinic for Cancer and Ageing (MCCA) at the Netherlands Cancer Institute (NKI) and Georgina Lakner, and Fabiana Steck for their help at the Vetsuisse Faculty mouse facility. We would like to also thank Ben Floot from the NKI for providing us with the NKI-A59 antibody, Dipanjan Chowdhury (Harvard Medical School, USA) for the pOZ-N-FH-IL2Rα plasmid, and Thomas J. Jentsch (Leibniz-Forschungsinstitut für Molekulare Pharmakologie (FMP) and Max-Delbrück-Centrum für Molekulare Medizin, D-13125 Berlin, Germany) for providing the rabbit polyclonal anti-LRRC8A/D antibodies. Moreover, we are grateful to Deborah Stroka, Tess Brodie and Joseena Iype from the Imaging Mass Cytometry and Mass Cytometry Platform (University of Bern) for their support with the CyTOF measurements. Financial support came from the Swiss National Science Foundation (310030_179360 to S.R., R'Equip 316030_183501), the European Union (ERC-2019-AdG-883877 to S.R. and TransCure - International Fellowship Program to N.D.), the Swiss Cancer League (KFS-5519-02-2022 to S.R.), and the Wilhelm-Sander Foundation (no. 2019.069.1 to S.R.).

## Author Contributions

C.W., I.K., N.D. performed the majority of the experiments and further data analysis under the supervision of S.R.. D.H. assisted with the *in vitro* experiments. M.D., C.G., M.S., N.RS., M.v.d.V., and R.d.KG. assisted with the *in vivo* experiments. J.A.G. performed the antibody protocol establishment and histological stainings. C.P. and I.H. generated the *Lrrc8d*$^{-/-}$ mice. T.J. provided the LRRC8A and LRRC8D antibodies. Z.N. and W.F. provided the ovarian cancer dataset analysis. C.V. and P.E. performed the HNSCC dataset analysis. C.W. and S.R. wrote the manuscript and all authors contributed with the critical reading and feedback of the manuscript.

## Declaration of Interests

The authors declare no competing interests.

691 **References**


692 1. Kelland L. The resurgence of platinum-based cancer chemotherapy. Nat Rev Cancer
693 2007;7:573–84.

694 2. Rottenberg S, Disler C, Perego P. The rediscovery of platinum-based cancer therapy. Nat Rev
695 Cancer 2021;21:37–50.

696 3. Pujade-Lauraine E, Fujiwara K, Ledermann JA, Oza AM, Kristeleit R, Ray-Coquard IL, et al.
697 Avelumab alone or in combination with chemotherapy versus chemotherapy alone in platinum-
698 resistant or platinum-refractory ovarian cancer (JAVELIN Ovarian 200): an open-label, three-
699 arm, randomised, phase 3 study. Lancet Oncol 2021;22:1034–46.

700 4. Burtness B, Harrington KJ, Greil R, Soulières D, Tahara M, de Castro G, et al. Pembrolizumab
701 alone or with chemotherapy versus cetuximab with chemotherapy for recurrent or metastatic
702 squamous cell carcinoma of the head and neck (KEYNOTE-048): a randomised, open-label,
703 phase 3 study. Lancet 2019;394:1915–28.

704 5. Gandhi L, Rodríguez-Abreu D, Gadgeel S, Esteban E, Felip E, De Angelis F, et al.
705 Pembrolizumab plus Chemotherapy in Metastatic Non-Small-Cell Lung Cancer. N Engl J Med
706 2018;378:2078–92.

707 6. Lippard SJ. New chemistry of an old molecule: cis-[Pt(NH3) 2Cl2]. Science; 1982;218:1075–
708 82.

709 7. Lord CJ, Ashworth A. The DNA damage response and cancer therapy. Nature 2012;481:287–
710 94.

711 8. Melinda LT, Kirsten MT, Julia R, Bryan H, Gordon BM, Kristin CJ, et al. Homologous
712 recombination deficiency (hrd) score predicts response to platinum-containing neoadjuvant
713 chemotherapy in patients with triple-negative breast cancer. Clin Cancer Res 2016;22:3764–
714 73.

715 9. Vollebergh MA, Lips EH, Nederlof PM, Wessels LFAA, Schmidt MK, van Beers EH, et al. An
716 aCGH classifier derived from BRCA1-mutated breast cancer and benefit of high-dose platinum-
717 based chemotherapy in HER2-negative breast cancer patients. Ann Oncol 2011;22:1561–70.

718 10. Vollebergh MA, Lips EH, Nederlof PM, Wessels LFAA, Wesseling J, vd Vijver MJ, et al.

719 Genomic patterns resembling BRCA1- and BRCA2-mutated breast cancers predict benefit of
720 intensified carboplatin-based chemotherapy. Breast Cancer Res 2014;16:R47.

721 11. Silver DP, Richardson AL, Eklund AC, Wang ZC, Szallasi Z, Li Q, et al. Efficacy of neoadjuvant
722 cisplatin in triple-negative breast cancer. J Clin Oncol 2010;28:1145–53.

723 12. Rottenberg S, Nygren AOHH, Pajic M, van Leeuwen FWBB, van der Heijden I, van de
724 Wetering K, et al. Selective induction of chemotherapy resistance of mammary tumors in a
725 conditional mouse model for hereditary breast cancer. Proc Natl Acad Sci U S A
726 2007;104:12117–22.

727 13. Rottenberg S, Jaspers JE, Kersbergen A, Van Der Burg E, Nygren AOHH, Zander SALL, et al.
728 High sensitivity of BRCA1-deficient mammary tumors to the PARP inhibitor AZD2281 alone
729 and in combination with platinum drugs. Proc Natl Acad Sci U S A. 2008;105:17079–84.

730 14. Keener AB. Innovative therapies to tackle platinum-resistant ovarian cancer. Nature
731 2021;600:S45–7.

732 15. Borst P, Rottenberg S, Jonkers J. How do real tumors become resistant to cisplatin? Cell Cycle
733 2008;7: 1353–9.

734 16. Borst P. Cancer drug pan-resistance: pumps, cancer stem cells, quiescence, epithelial to
735 mesenchymal transition, blocked cell death pathways, persisters or what? Open Biol
736 2012;2:120066–120066.

737 17. Edwards SL, Brough R, Lord CJ, Natrajan R, Vatcheva R, Levine DA, et al. Resistance to
738 therapy caused by intragenic deletion in BRCA2. Nature 2008;451:1111–5.

739 18. Sakai W, Swisher EM, Karlan BY, Agarwal MK, Higgins J, Friedman C, et al. Secondary
740 mutations as a mechanism of cisplatin resistance in BRCA2-mutated cancers. Nature
741 2008;451:1116–20.

742 19. Patch AM, Christie EL, Etemadmoghadam D, Garsed DW, George J, Fereday S, et al. Whole-
743 genome characterization of chemoresistant ovarian cancer. Nature 2015;521:489–94.

744 20. Burger H, Loos WJ, Eechoute K, Verweij J, Mathijssen RHJ, Wiemer EAC. Drug transporters of
745 platinum-based anticancer agents and their clinical significance. Drug Resist Updat
746 2011;14:22–34.

21. Planells-Cases R, Lutter D, Guyader C, Gerhards NM, Ullrich F, Elger DA, et al. Subunit composition of VRAC channels determines substrate specificity and cellular resistance to Pt-based anti-cancer drugs. EMBO J. 2015;34:2993–3008.

22. Qiu Z, Dubin AE, Mathur J, Tu B, Reddy K, Miraglia LJ, et al. SWELL1, a plasma membrane protein, is an essential component of volume-regulated anion channel. Cell 2014;157:447–58.

23. Trothe J, Ritzmann D, Lang V, Scholz P, Pul Ü, Kaufmann R, et al. Hypotonic stress response of human keratinocytes involves LRRC8A as component of volume-regulated anion channels. Exp Dermatol 2018;27:1352–60.

24. Voss FK, Ullrich F, Muñch J, Lazarow K, Lutte D, Mah N, et al. Identification of LRRC8 heteromers as an essential component of the volume-regulated anion channel VRAC. Science 2014;344:634–8.

25. Jaspers JE, Kersbergen A, Boon U, Sol W, van Deemter L, Zander SA, et al. Loss of 53BP1 causes PARP inhibitor resistance in BRCA1-mutated mouse mammary tumors. Cancer Discov 2013;3:68–81.

26. Duarte AA, Gogola E, Sachs N, Barazas M, Annunziato S, R de Ruiter J, et al. BRCA-deficient mouse mammary tumor organoids to study cancer-drug resistance. Nat Methods 2018;15:134–40.

27. Harmsen T, Klaasen S, Van De Vrugt H, Te Riele H. DNA mismatch repair and oligonucleotide end-protection promote base-pair substitution distal from a CRISPR/Cas9-induced DNA break. Nucleic Acids Res 2018;46:2945–55.

28. Brinkman EK, Chen T, Amendola M, Van Steensel B. Easy quantitative assessment of genome editing by sequence trace decomposition. Nucleic Acids Res 2014;42:e168

29. Guzmán C, Bagga M, Kaur A, Westermarck J, Abankwa D. ColonyArea: An ImageJ Plugin to Automatically Quantify Colony Formation in Clonogenic Assays. Rota R, editor. PLoS One 2014;9:e92444.

30. Pritchard CEJ, Kroese LJ, Huijbers IJ. Direct generation of conditional alleles using CRISPR/Cas9 in mouse zygotes. Methods Mol Biol 2017;1642: 21–35.

31. Terheggen PMAB, Floot BGJ, Lempers ELM, Van Tellingen O, Begg AC, Den Engelsel L.

Antibodies against eisplatin-modified DNA and cisplatin-modified (di)nueleotides. Cancer Chemother Pharmacol. 1991; 28:185-91.

32. Giesen C, Wang HAO, Schapiro D, Zivanovic N, Jacobs A, Hattendorf B, et al. Highly multiplexed imaging of tumor tissues with subcellular resolution by mass cytometry. Nat Methods 2014;11:417–22.

33. Chang Q, Ornatsky OI, Siddiqui I, Straus R, Baranov VI, Hedley DW. Biodistribution of cisplatin revealed by imaging mass cytometry identifies extensive collagen binding in tumor and normal tissues. Sci Rep 2016;6:36641.

34. Schindelin J, Arganda-Carreras I, Frise E, Kaynig V, Longair M, Pietzsch T, et al. Fiji: an open-source platform for biological-image analysis. Nat Methods 2012;9:676–82.

35. Essers PBM, van der Heijden M, Vossen D, de Roest RH, Leemans CR, Brakenhoff RH, et al. Ovarian cancer-derived copy number alterations signatures are prognostic in chemoradiotherapy-treated head and neck squamous cell carcinoma. Int J Cancer 2020;147:1732–9.

36. van der Heijden M, Essers PBM, Verhagen CVM, Willems SM, Sanders J, de Roest RH, et al. Epithelial-to-mesenchymal transition is a prognostic marker for patient outcome in advanced stage HNSCC patients treated with chemoradiotherapy. Radiother Oncol 2020;147:186–94.

37. Yoshihara K, Tsunoda T, Shigemizu D, Fujiwara H, Hatae M, Fujiwara H, et al. High-risk ovarian cancer based on 126-gene expression signature is uniquely characterized by downregulation of antigen presentation pathway. Clin Cancer Res 2012;18:1374–85.

38. Pajic M, Blatter S, Guyader C, Gonggrijp M, Kersbergen A, Küçükosmanoğlu A, et al. Selected alkylating agents can overcome drug tolerance of G 0 -like tumor cells and eradicate BRCA1-deficient mammary tumors in mice. Clin Cancer Res 2017;23:7020–33.

39. Lee CC, Freinkman E, Sabatini DM, Ploegh HL. The protein synthesis inhibitor blasticidin s enters mammalian cells via Leucine-rich repeat-containing protein 8D. J Biol Chem 2014;289:17124–31.

40. Crona DJ, Faso A, Nishijima TF, McGraw KA, Galsky MD, Milowsky MI. A Systematic Review of Strategies to Prevent Cisplatin-Induced Nephrotoxicity. Oncologist 2017;22:609–19.

41. Liu X, Holstege H, van der Gulden H, Treur-Mulder M, Zevenhoven J, Velds A, et al. Somatic loss of BRCA1 and p53 in mice induces mammary tumors with features of human BRCA1-mutated basal-like breast cancer. Proc Natl Acad Sci U S A. 2007;104:12111–6.

42. Kumar L, Chou J, Yee CSK, Borzutzky A, Vollmann EH, von Andrian UH, et al. Leucine-rich repeat containing 8A (LRRC8A) is essential for T lymphocyte development and function. J Exp Med 2014;211:929–42.

43. Strojan P, Vermorken JB, Beitler JJ, Saba NF, Haigentz M, Bossi P, et al. Cumulative cisplatin dose in concurrent chemoradiotherapy for head and neck cancer: A systematic review. Head Neck 2016;38:E2151–8.

44. Al-Mamgani A, de Ridder M, Navran A, Klop WM, de Boer JP, Tesselaar ME. The impact of cumulative dose of cisplatin on outcome of patients with head and neck squamous cell carcinoma. Eur Arch Otorhinolaryngol. Eur Arch Otorhinolaryngol 2017;274:3757–65.

45. Safaei R, Howell SB. Copper transporters regulate the cellular pharmacology and sensitivity to Pt drugs. Crit Rev Oncol Hematol. Crit Rev Oncol Hematol 2005;53:13–23.

46. Hall MD, Okabe M, Shen DW, Liang XJ, Gottesman MM. The role of cellular accumulation in determining sensitivity to platinum-based chemotherapy. Annu Rev Pharmacol Toxicol 2008;48:495–535.

47. Filipski KK, Mathijssen RH, Mikkelsen TS, Schinkel AH, Sparreboom A. Contribution of organic cation transporter 2 (OCT2) to cisplatin-induced nephrotoxicity. Clin Pharmacol Ther 2009;86:396–402.

48. Ciarimboli G, Deuster D, Knief A, Sperling M, Holtkamp M, Edemir B, et al. Organic cation transporter 2 mediates cisplatin-induced oto- and nephrotoxicity and is a target for protective interventions. Am J Pathol 2010;176:1169–80.

49. Komatsu M, Sumizawa T, Mutoh M, Chen ZS, Terada K, Furukawa T, et al. Copper-transporting P-type adenosine triphosphatase (ATP7B) is associated with cisplatin resistance. Cancer Res 2000. 60:1312–6.

50. Gately DP, Howell SB. Cellular accumulation of the anticancer agent cisplatin: a review. Br J Cancer 1993;67:1171–6.

51. He YJ, Meghani K, Caron M-CC, Yang C, Ronato DA, Bian J, et al. DYNLL1 binds to MRE11 to limit DNA end resection in BRCA1-deficient cells. Nature 2018;563:522–6.

52. Abascal F, Zardoya R. LRRC8 proteins share a common ancestor with pannexins, and may form hexameric channels involved in cell-cell communication. BioEssays 2012;34:551–60.

53. Nakamura R, Numata T, Kasuya G, Yokoyama T, Nishizawa T, Kusakizako T, et al. Cryo-EM structure of the volume-regulated anion channel LRRC8D isoform identifies features important for substrate permeation. Commun Biol 2020;3:240.

54. Kasuya G, Nakane T, Yokoyama T, Jia Y, Inoue M, Watanabe K, et al. Cryo-EM structures of the human volume-regulated anion channel LRRC8. Nat Struct Mol Biol 2018;25:797–804.

55. Ruprecht N, Hofmann L, Hungerbühler MN, Kempf C, Heverhagen JT, von Tengg-Kobligk H. Generation of Stable cisPt Resistant Lung Adenocarcinoma Cells. Pharmaceuticals (Basel). 2020;13:1–18.

56. Lück JC, Puchkov D, Ullrich F, Jentsch TJ. LRRC8/VRAC anion channels are required for late stages of spermatid development in mice. J Biol Chem 2018;293:11796–808.

**Figure 1 Loss of *Lrrc8a* or *Lrrc8d* induces Pt-drug resistance in BRCA1;p53-deficient mammary tumor cells A)** Representative Western blots of control (ntg B1 and ntg C1), *Lrrc8a* (*Lrrc8a*_C10 and *Lrrc8a*_D8) and *Lrrc8d* (*Lrrc8d*_E12 and *Lrrc8d*_G12) knockout cell lines used in the validation experiments. **B)** Proliferation rates of wild type and *Lrrc8a* or *Lrrc8d* knockout cells. Mean ± SD of six replicates is shown. **C-H** Clonogenic survival assays and quantification of wild type and LRRC8A/D-deficient cell lines treated with cisplatin (C+D), carboplatin (E+F), or oxaliplatin (G+H). Representative images of selected lines and concentrations are shown. Data represent mean ± SD of three independent replicates and were fitted to a four parameter logistic (4PL) sigmoidal curve. *P*-values are calculated by one-way ANOVA followed by Tukey's multiple comparisons test for the log(IC50) values of the survival curves ****$p$<0.0001. **I-L)** Quantification of clonogenic growth assays using the different *Lrrc8a* (*Lrrc8a*_D8 + pOZ empty, + pOZ *Lrrc8a* wt polyclonal or clonal lines) or *Lrrc8d* (*Lrrc8d*_D8 + pOZ empty, + pOZ *Lrrc8d* wt polyclonal or clonal lines) rescue cell lines treated with cisplatin or carboplatin. As negative controls, empty vector-transduced cell lines were used. Data represent mean ± SD of three independent replicates and were fitted to a four parameter logistic (4PL) sigmoidal curve. *P*-values are calculated by one-way ANOVA followed by Tukey's multiple comparisons test for the log(IC50) values of the survival curves. ****$p$<0.0001, **$p$<0.01. **M)** Representative images of selected conditions of the clonogenic growth assays in the presence of cisplatin or carboplatin, using the rescue cell lines from **I-L** are shown.

**Figure 2 Loss of *Lrrc8a* or *Lrrc8d* reduces cisplatin uptake and the subsequent formation of Pt-DNA adducts and DNA damage. A)** CyTOF-based measurement of Pt uptake over time using 0.5μM cisplatin in non-targeting (ntg) control, *Lrrc8a-,* or *Lrrc8d*-knockout cell lines. The data represents the mean ± SD of three independent replicates consisting of three technical replicates each, where approximately 100'000 cells per condition and cell lines were acquired (two-way ANOVA followed by Tukey's multiple comparisons test, ****$p$<0.0001, **$p$<0.01). **B)** CyTOF-based measurement of Pt uptake after 24h treatment with 4μM carboplatin of ntg, *Lrrc8a-,* or *Lrrc8d*-knockout cell lines. The data represents the mean ± SD of three independent replicates where approximately 50'000 cells per condition and cell lines were acquired (two-way ANOVA followed by Tukey's multiple comparisons test, ****$p$<0.0001). **C)** CyTOF-based measurement of Pt uptake after 24h treatment with 0.5μM cisplatin, 4μM carboplatin or 0.5μM oxaliplatin of selected clonal *Lrrc8a-,* or *Lrrc8d-* high expression rescue lines compared to the empty vector transduced knockout cell line. The data represents the mean ± SD of three independent replicates where approximately 50'000 cells per condition and cell lines were acquired (two-way ANOVA followed by Tukey's multiple comparisons test, ****$p$<0.0001). **D)** Representative images of the average nuclear staining in ntg or *Lrrc8a* or *Lrrc8d*-knockout cell lines using the NKI-A59 antibody against cisplatin-adducts in the presence or absence of 10μM cisplatin treatment for 6h; the scale bar represents 10μm. **E)** Quantification of the raw integrated density per nucleus of the NKI-A59 cisplatin adduct staining, mean with ± 95% confidence interval of three independent replicates are shown. Per replicate approximately 100 nuclei were quantified. The significance was determined using two-way ANOVA followed by Tukey's multiple comparison test. ****$p$<0.0001 **F)** Representative images of yH2AX immunofluorescence staining of *Lrrc8a*$^{-/-}$, *Lrrc8d*$^{-/-}$, and control cell lines following cisplatin treatment. The scale bar represents 20μm. **G)** Quantification of yH2AX foci in the nucleus of *Lrrc8a*$^{-/-}$, *Lrrc8d*$^{-/-}$ and control cell lines in response to cisplatin treatment. Per cell line and condition, 200 nuclei were quantified each replicate. Median ± 95% confidence interval of three independent replicates are shown (ordinary one-way ANOVA followed by Tukey's multiple comparisons test, ****$p$<0.0001).

888 **Figure 3 *Lrrc8a* and *Lrrc8d* deficiency promote carboplatin resistance *in vivo* A)** Schematic over-
889 view of the *in vivo* experiment **B-C)** Kaplan-Meyer overall survival curves of mice transplanted with
890 LRRC8A/D-deficient or ntg control tumors treated with either vehicle or 50 mg/kg carboplatin. Statistical
891 analysis was performed with the log-rank test (Mantel-Cox). *$p < 0.05$, ***$p < 0.001$

**Figure 4 Cisplatin uptake into the kidneys of LRRC8D-deficient mice and subsequent DNA damage are reduced. A)** A schematic overview of the development of *Lrrc8d* KO mice using CRISPR/Cas9-mediated knockout of the first coding exon (2561 bp) in zygotes. **B)** Western blotting of LRRC8D using kidney lysates derived from wild type, heterozygous and homozygous *Lrrc8d* knockout mice. **C)** Representative images of the IMC tissue analysis of cisplatin- or vehicle-treated wild type or LRRC8D-deficient mice. For the illustration, the most abundant isotope $^{194}Pt$ was used. For the visualization of the nuclei within the tissue, the signal of the iridium DNA intercalator isotope $^{191}Ir$ is shown. Highlighted are 3 image sections which were used for the quantification of the mean Pt levels. The scale bar represents 200µm. **D)** Normalized mean $^{194}Pt$ kidney measurements of wild type or LRRC8D deficient mice, 6h after treatment with 6mg cisplatin per kg *i.v.* or the vehicle. Three 1mm$^2$ sections of 3 kidneys per group were acquired, where three image sections from the cortical region of each acquisition were quantified. This results in 27 data points per group. The data represent the $^{134}Xe^+$ normalized mean $^{194}Pt$ signal of the image sections ± SD (two-way ANOVA, followed by Tukey's multiple comparisons test). **E)** Immunohistochemistry using the anti-cisplatin-DNA adduct and anti-yH2AX antibodies of wild type, heterozygous and homozygous *Lrrc8d* knockout mice after the treatment with 6 mg cisplatin per kg for 6 hours. The images were taken at 40x magnification. The scale bar represents 50µm. **F+G)** The percentage of positive nuclei in 50 kidney cortex image sections per kidney (for NKI-A59 antibody) or the whole cortical kidney region of each mouse (for yH2AX) were quantified and normalized via the average basal levels of the untreated samples; vehicle: wt N=5, het KO N=8, hom KO N=8, treated: wt N=8, het KO N=12, hom KO N=16, ****$p$<0.0001. The data represent mean percentage of positive nuclei over all the image sections per mouse ± SD (two-way ANOVA, followed by Tukey's multiple comparisons test). **H+I)** Kaplan-Meyer relapse free survival of mice transplanted with either cisplatin-naïve tumors (H) or cisplatin resistant tumors (I). The mice were treated on day 0 and day 14 with the indicated dose of cisplatin (*i.v*). For the treatment with 12 mg/kg *i.v.* the *Lrrc8d* KO mice were used. Statistical analysis was performed with the log-rank test (Mantel-Cox). **$p$ < 0.01, ***$p$ < 0.001

**Figure 5 Loss of *LRRC8A* or *LRRC8D* reduces survival parameters in head and neck squamous cell carcinoma patients treated with a chemoradiotherapy regimen. A)** Overall survival, progression, locoregional control, and distant metastasis parameters of patients with at least -1 *LRRC8A* copy number loss versus control **B)** Comparison of polyA RNA sequencing expression data to copy number loss of *LRRC8A*. Patients were classified into "low" expression group by the cutoff at around 20 rpkm **C)** Overall survival data of high (N=129) and low (N=58) *LRRC8A* expressing patients defined by the cutoff determined in B. **D)** Patients were further classified into received cumulative dose groups of below or above 200 mg/m$^2$ of cisplatin. **E)** Correlation analysis of *LRRC8A* versus *LRRC8D* expression levels. **F)** Overall survival, progression, and locoregional control parameters of patients differentially expressing *LRRC8D* (low N=61, medium N=60, high =60) **G)** Distant metastasis outcome of patients with low, medium or high *LRRC8D* expression. **H)** Distant metastasis outcome of patients differentially expressing *LRRC8D* further classified in high cumulative dose (left) and low cumulative dose of cisplatin (right). **I)** Forest plots displaying the results from CoxPH model fits for OS, PFS, locoregional control and DM-free survival for the >200 mg/m$^2$ of cisplatin or <200 mg/m$^2$ of cisplatin treatment groups.

Figure 1

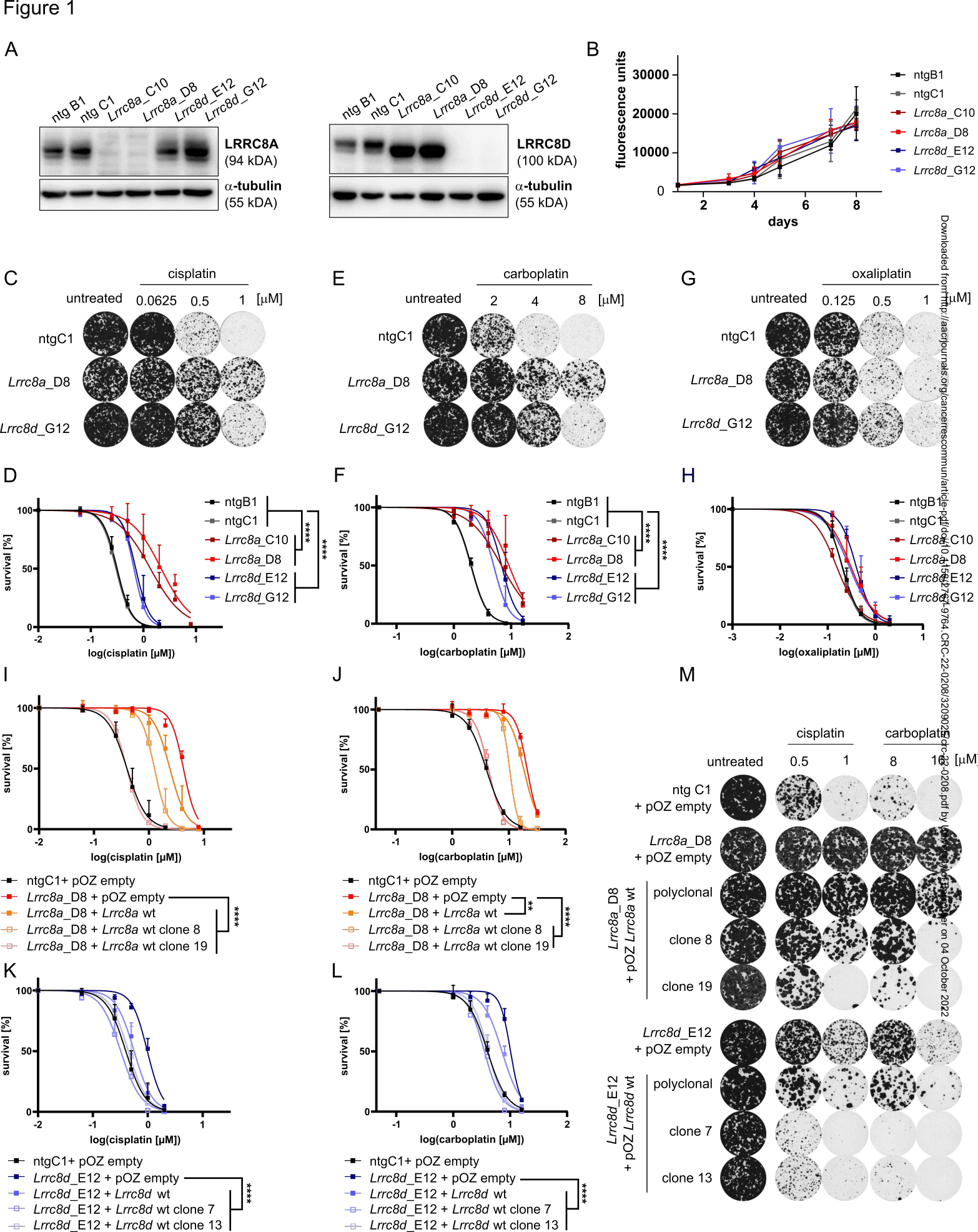

Figure 2

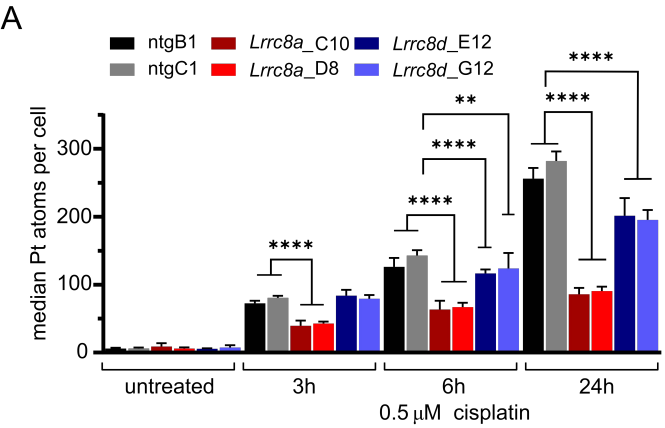


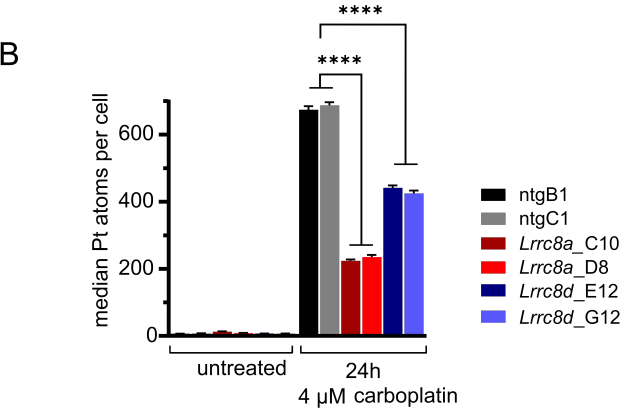


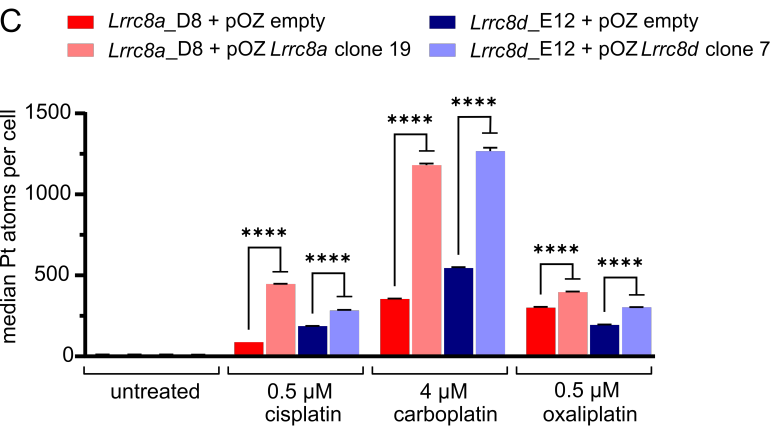


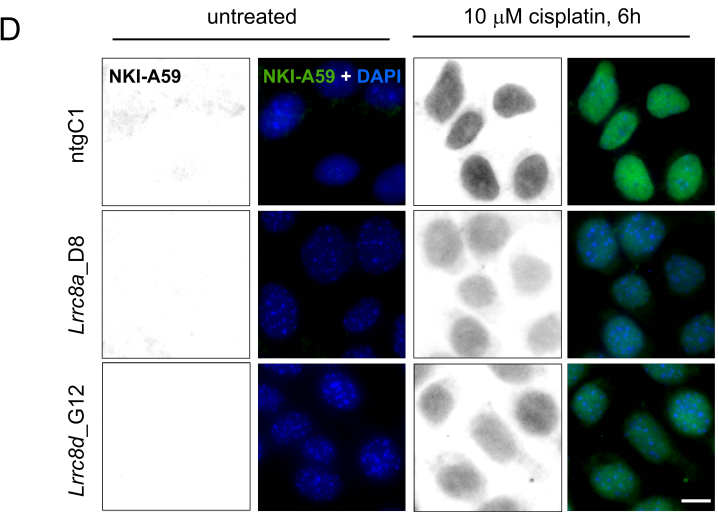


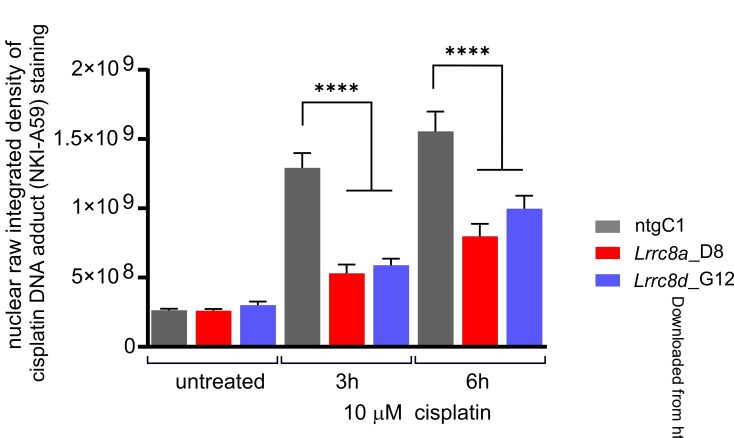


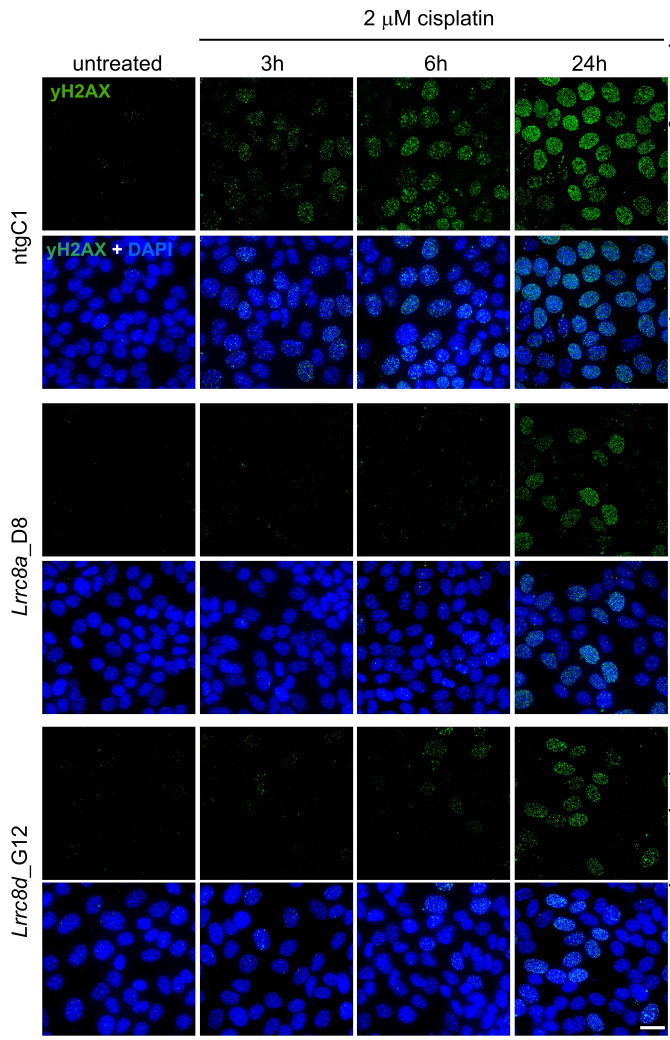


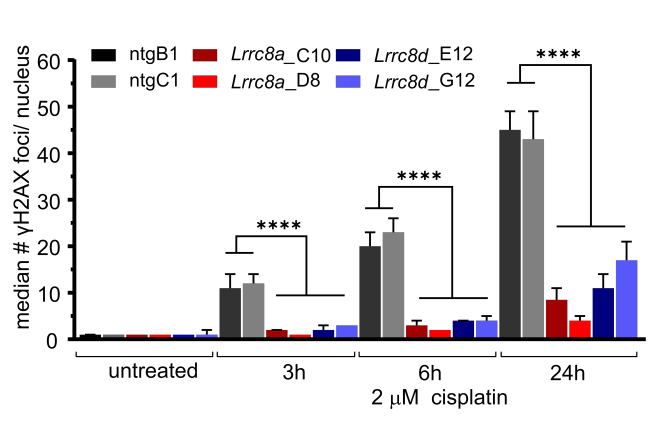

Figure 3

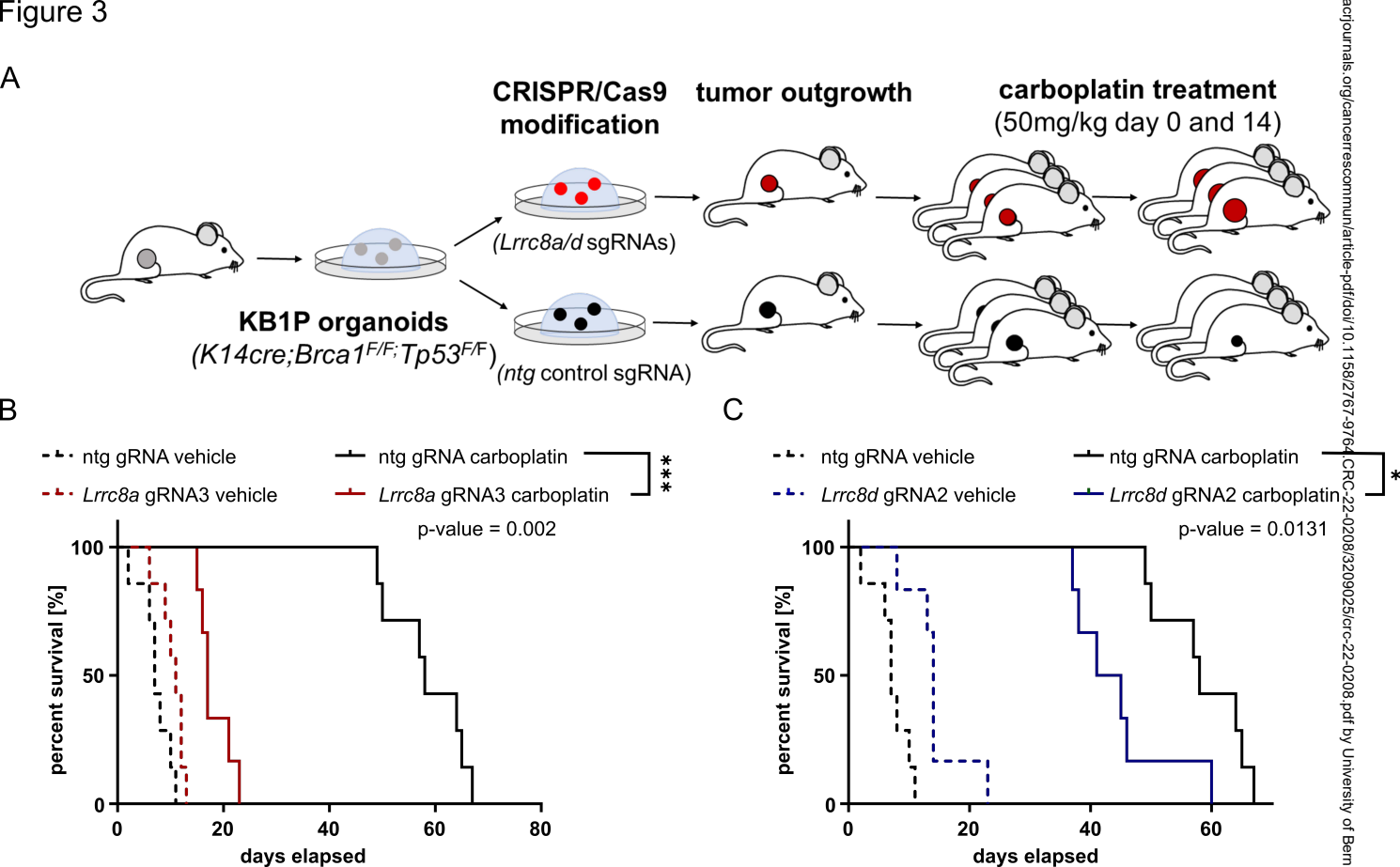

Figure 4

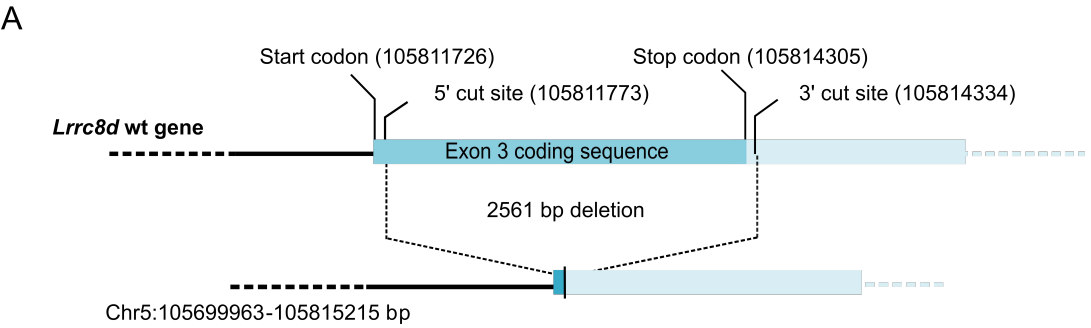


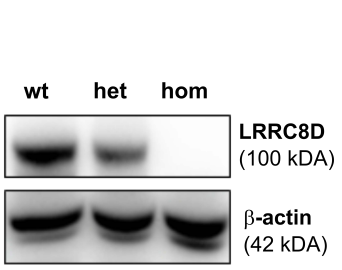


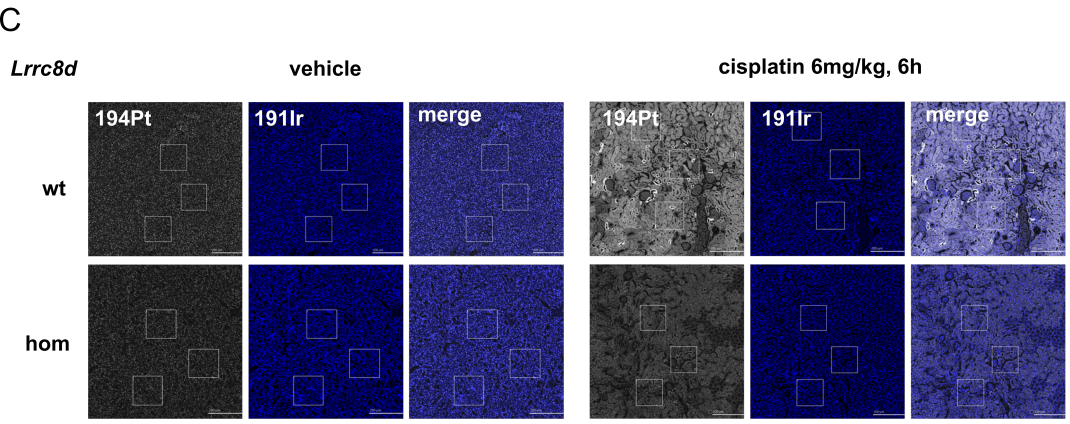


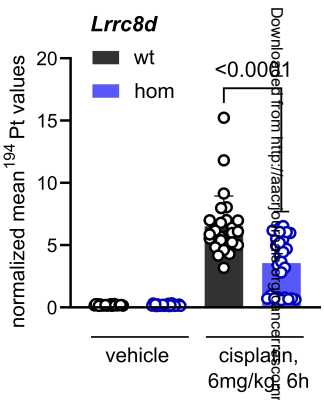


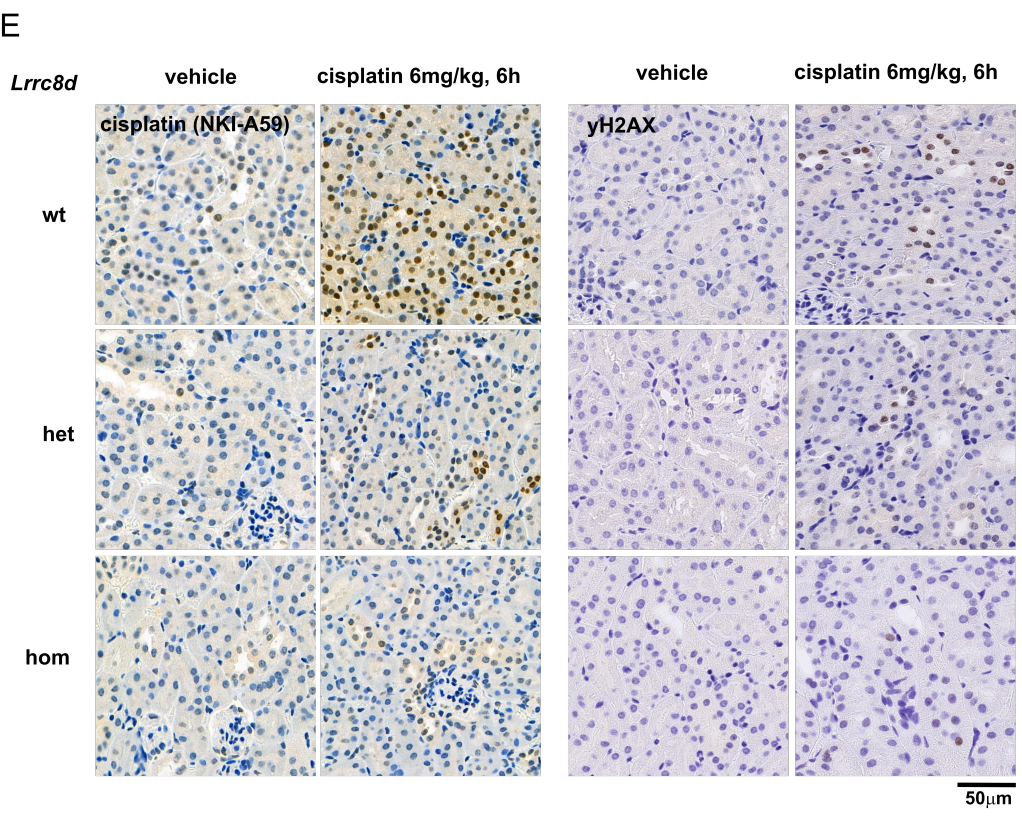


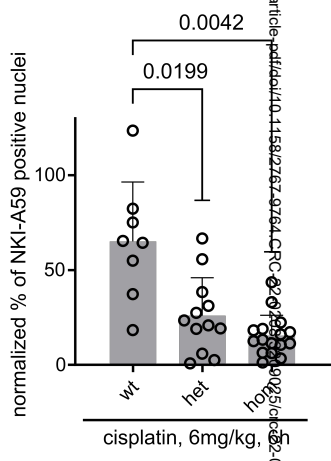


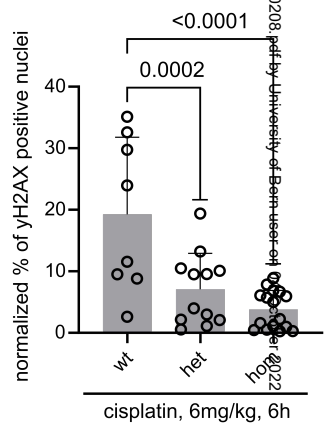


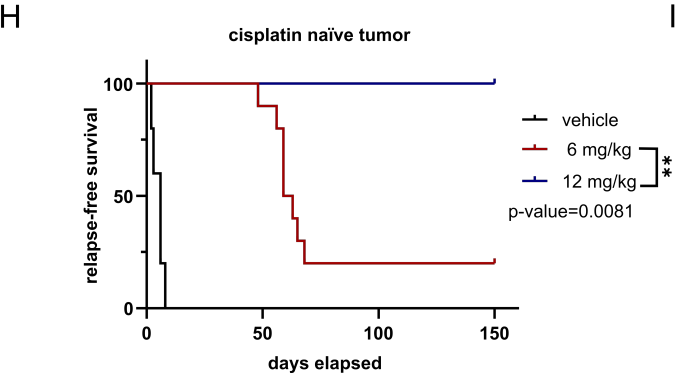


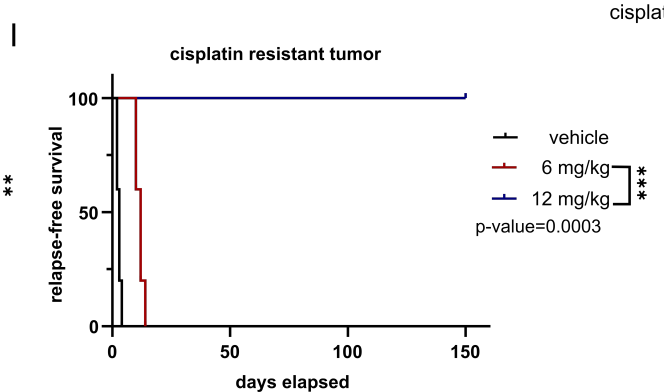

Figure 5